High ion-exchange capacity semi-homogeneous cation exchange membranes prepared via a novel polymerization and sulfonation approach in porous polypropylene

Shanxue Jiang,[†] Bradley P. Ladewig[*,†]

[†]Barrer Centre, Department of Chemical Engineering, Imperial College London, United Kingdom

ABSTRACT

Semi-homogeneous cation exchange membranes with superior ion exchange capacity (IEC) were synthesized via a novel polymerization and sulfonation approach in porous polypropylene support. The IEC of membranes could reach up to 3 mmol/g, due to high mass ratio of functional polymer to membrane support. Especially, theoretical IEC threshold value agreed well with experimental threshold value, indicating that IEC could be specifically designed without carrying out extensive experiments. Also, sulfonate groups were distributed both on membrane surface and across the membranes, which corresponded well with high IEC of the synthesized membranes. Besides, the semi-finished membrane showed hydrophobic property due to formation of polystyrene. In contrast, the final membranes demonstrated super hydrophilic property, indicating the adequate sulfonation of polystyrene. Furthermore, when sulfonation reaction time increased, the conductivity of membranes also showed a tendency to increase, revealing the positive relationship between conductivity and IEC. Finally, the final membranes showed sufficient thermal stability for electrodialysis applications such as water desalination.

KEYWORDS: cation exchange membrane, electrodialysis, ion exchange capacity, water contact angle, thermal properties

1. INTRODUCTION

Ion exchange membranes (IEMs) are widely used in various fields, including but not limited to electrodialysis (ED),[1,2] reverse electrodialysis (RED),[3] diffusion dialysis,[4] fuel cells,[5,6] and redox flow battery.[7] Especially, ED is extensively applied in a number of applications, such as water treatment and desalination,[8] food industry,[9] and so on. The widespread applications of IEMs also necessitate different methods for synthesizing IEMs with different properties to meet different requirements.[10–12] For example, U. Chatterjee et al. reported a novel kind of ion exchange membrane via quaternization and cross-linking methods which demonstrated high current efficiency and low energy consumption.[13] Also, the widely used carcinogenic reagent (i.e., chloromethyl ether) was avoided during the preparation process.[14] However, many methods or procedures have one or more of the following issues: use of organic solvents,[15,16] use of additional chemicals to improve solubility of effective reactants or functional components,[17] heterogeneous casting solution,[18] complicated procedures,[19] reduced membrane long-term stability,[20] etc. This paper aimed to provide a solution to these issues.

In terms of ionic group types, IEMs are generally divided into cation exchange membranes and anion exchange membranes.[21,22] Ideally, IEMs are supposed to have high permselectivity, high conductivity, high ion exchange capacity (IEC) as well as reliable chemical, mechanical, and thermal stabilities.[22–26] Among these properties, IEC is undoubtedly an important parameter for IEMs. In industrial ED applications, electricity consumption is a main source of operation cost. Increasing IEC can reduce electricity consumption by increasing the output of desalted water per kilowatt hour. Membranes with low IEC usually have high area resistance, resulting high electricity cost as well as long processing time due to low efficiency.[27] However, it was not easy to prepare membranes with high IEC. K. Dutta et al. prepared high ion-exchange capacity Nafion membranes through casing blend solutions of Nafion and sulfonated polyaniline and the synthesized membranes demonstrated improved ion exchange capacity (1.43 mmol/g) compared to pristine Nafion (0.8 mmol/g).[28] X. Li et al. synthesized novel high ion-exchange capacity proton exchange membranes using ring-opening metathesis polymerization and the IEC could reach up to 2.3 mmol/g.[29] However, besides the complicated procedures, solution casting method was adopted in these procedures, where organic solvents were used, which may pose a threat to the environment.

In this work, we proposed a novel methodology for making high ion-exchange capacity cation exchange membranes through controlling the mass ratio of functional polymers to membrane support. The inspiration for this methodology was originated from formation of reinforced concrete, one of the most widely used modern building materials. As illustrated in Figure 1, the interconnected rebar provides solid support for concrete, and the former is filled with the latter, resulting reinforced concrete after solidification of concrete slurry. Similarly, membranes fabricated using this methodology is composed of two parts. The first part is membrane support and the second part is functional polymers. The relationship between membrane support and the functional polymers is analogous to that of rebar and concrete in reinforced concrete. Specifically, membrane support should have strong chemical, mechanical

and thermal stability. More importantly, it should also have porous structure (voids) and low density, thus making it possible to have high liquid uptake capacity and to provide enough space for functional polymers as well. In other words, the secret of high IEC produced using this methodology lies in high amount of functional polymers introduced to the synthesized membranes. Briefly, the functional polymers are formed by functionalization of polymers and the polymers are formed by polymerization of monomers. Especially, all the reactions take place in the membrane support. Therefore, the finally formed functional polymers are closely interconnected with membrane support. In this study, non-woven polypropylene (PP) support fabric Novatexx 2471 was used as membrane support, which had a porous structure as revealed by the SEM image (Figure 1C), and high liquid uptake capacity. Sulfonated polystyrene (PSS) was used as functional polymers, which was formed by sulfonation of crosslinked polystyrene (PS) that "grew up" in the membrane support through polymerization of styrene and divinylbenzene (Figure 1D). Not limited to PS/PSS and PP, this methodology may also be applied to other combinations and anion exchange membranes as well. Therefore, this methodology may provide an avenue for future research work on IEMs with high IEC.

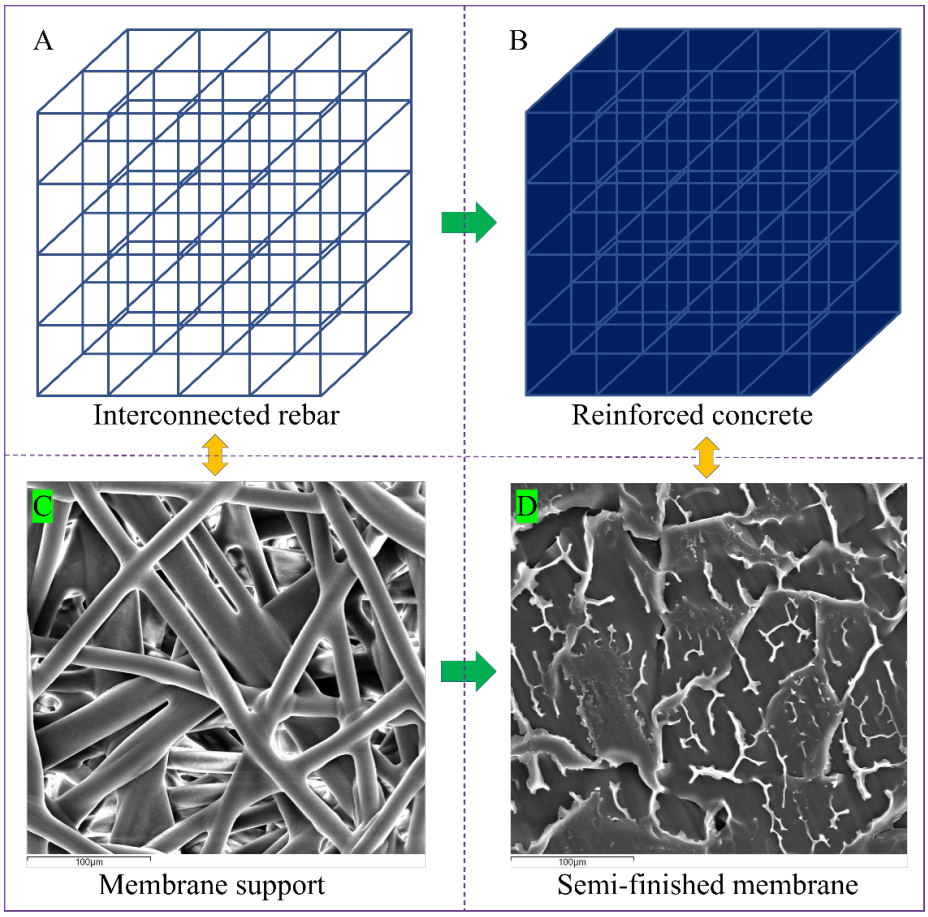


Figure 1. Conceptual illustration of the methodology in this study. (A) Interconnected rebar (B) Schematic diagram of reinforced concrete (C) SEM image of membrane support used in this study (D) SEM image of semi-finished membrane in this study

2. EXPERIMENTAL SECTION

2.1. Materials. Styrene, divinylbenzene, benzoyl peroxide, sodium chloride, and phenolphthalein solution were purchased from Sigma Aldrich. Non-woven polypropylene (PP) support fabric Novatexx 2471 was supplied by Freudenberg Filtration Technologies (Germany). All chemicals were used as received without any further purification.

2.2. Membrane preparation. The membrane preparation scheme was illustrated in Figure 2. To begin with, styrene (St), divinylbenzene (DVB) and benzoyl peroxide (BPO) with mass ratio of 7:1:0.07 were mixed together at room temperature, and the mixture was then stirred moderately at room temperature to make homogeneous solution. Then PP membrane support was immersed into the solution for at least 10 min to ensure adequate uptake of the solution. Then the PP membrane was taken out and placed between two Aluminium sheets, and then the Aluminium sheets were sandwiched between two stainless steel plates. The stainless-steel plates were then compressed tightly to prevent monomers from escaping PP membrane and to ensure that polymerization took place in the membrane support. The polymerization took place at 80°C for 8 hours. After the reaction, the membrane was peeled off and immersed into acetone or heated at 60°C for several hours to remove unreacted monomers. Then the membrane was immersed into concentrated sulfuric acid and the sulfonation reaction took place at 80°C for different hours. After the reaction, the membrane was taken out and immersed into ice-water mixture to remove excess acid. Then the membrane was washed with DI water for a couple of times to obtain final membranes.

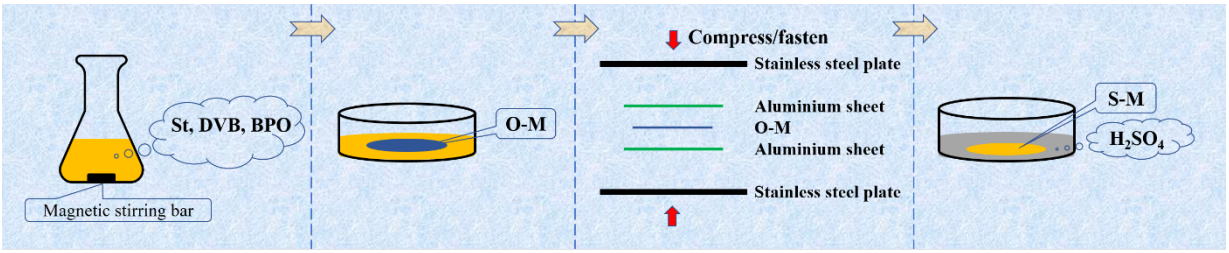


Figure 2. Schematic illustration of membrane preparation. O-M referred to original PP membrane support; S-M referred to semi-finished membrane synthesized by copolymerization of St and DVB in O-M.

2.3. Membrane characterization. Scanning electron microscope (SEM) analysis as well as energy-dispersive X-ray spectroscopy (EDS or EDX) analysis were performed (JSM 6400, JEOL, USA) to study membrane morphology as well as sulfur distribution in the synthesized membranes.

The molecular structure of synthesized membranes was characterized using Fourier-transform infrared spectroscopy (FTIR) technique (Perkin-Elmer, USA, model Spectrum-100). The FTIR spectra of the membrane samples were taken from 600 cm^{-1} to 4000 cm^{-1}.

IEC of membranes is often defined as the amount of exchangeable ions per dry weight of the membrane, with the unit of meq/g or mmol/g.[30] Titration method was adopted to determine IEC of the synthesized membranes.[31] In brief, the membrane (H^+ form) was immersed in 2 M NaCl solution for 24 hours to convert H^+ form into Na^+ form. During the conversion process, H^+ was released into the solution. The membrane sample was then taken out from the solution and completely washed with DI water, which was then mixed with the solution. Following this, the solution was titrated with 0.01 M NaOH using phenolphthalein as the indicator. The IEC of membranes could be calculated using the following equation:

$$\text{IEC} = \frac{CV}{W_{dry}} \qquad (1)$$

where C is the concentration of NaOH solution, V is the volume of NaOH solution consumed and W_{dry} is the dry weight of the membrane sample in H^+ form.

Water uptake was determined by two steps. Firstly, the membrane sample was dried at 60 ˚C under oven until the sample weight did not change any more. Secondly, the membrane sample was immersed in DI water for 24 h at room temperature, and then excess water on membrane sample was lightly removed with tissue, and then the weight of membrane sample was measured immediately. Water uptake was calculated using the following equation:

$$\text{Water uptake} = \frac{W_{wet} - W_{dry}}{W_{dry}} \qquad (2)$$

where W_{wet} and W_{dry} are wet weight and dry weight of the membrane, respectively.

Water contact angles of the synthesized membranes were determined by sessile-drop technique, using standard goniometer (Ramehart Instrument, USA, model 250-U1) equipped with a high-speed digital camera which operates at 100 fps.

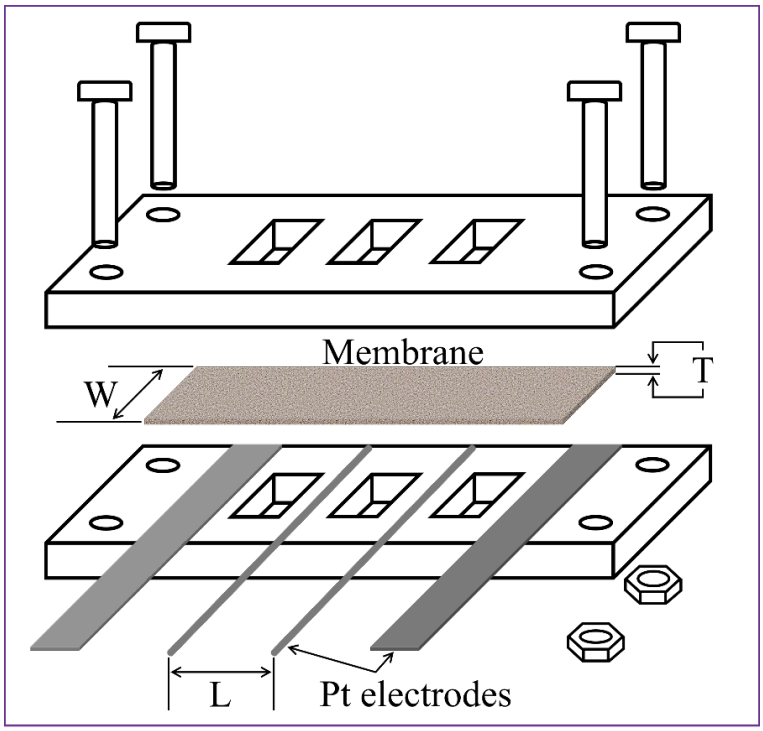


Figure 3. Schematic diagram of proton conductivity testing cell

The proton conductivity of synthesized membranes was determined using electrochemical impedance spectroscopy (EIS) technique and four-electrode in-plane proton conductivity testing method.[32–34] Figure 3 showed the schematic diagram of conductivity testing method. For the testing procedure, the membrane sample was placed into the testing device that was connected with BioLogic VSP potentiostat. The testing device was immersed into ultra-pure water (~18 MΩ·cm) at room temperature. Alternating current (AC) impedance data was collected in frequency range of 0.1 Hz to 1 MHz with a sinus amplitude of 100 mV across the electrodes. After the test, the membrane sample was taken out and the device was immersed into water again to measure background resistance. Membrane resistance was calculated using the following equation:[32,35]

$$R = \frac{R_t R_b}{R_b - R_t} \qquad (3)$$

where R is the membrane resistance, R_t is the total resistance (with membrane) and R_b is the background resistance (without membrane).

Membrane conductivity was then calculated using the following equation:[35]

$$\sigma = \frac{L}{RTW} \qquad (4)$$

where σ is membrane conductivity, L is the distance between the inner electrodes, T is membrane thickness and W is membrane width (Figure 3). More details about conductivity measurement were available in Supporting Information.

Thermogravimetric analysis (TGA) and differential scanning calorimetry (DSC) were used to study thermal stability of synthesized membranes. The test was conducted via a Netzsch

instrument (model STA 449 F5 Jupiter®) under nitrogen flow of 20 cm^3/min at a heating rate of 10 °C/min in the range of 25–800 °C.

3. RESULTS AND DISCUSSION

3.1. Membrane morphology and sulfur distribution

In this work membranes with different sulfonation reaction time were synthesized using the proposed novel methodology. Generally, surface morphology of synthesized membranes (i.e., S-M and F-M) was strongly influenced by preparation conditions. As revealed by Figure 1A, membrane support (i.e., O-M) had an intertwined porous structure (voids), which contributed greatly to its high liquid uptake capacity. Similar to the role of rebar in reinforced concrete, the intertwined porous structure enabled polymerization reaction to take place in O-M, producing compacted semi-finished membrane (S-M). As shown in Figure 1B, the voids in O-M were filled with crosslinked polystyrene (confirmed by FTIR), the role of which was similar to that of concrete in reinforced concrete. Also, it is interesting to mention that the surface of S-M was not smooth, which might be attributed to a synthetic effect of multi-factors, including the porous structure of O-M, surface smoothness of the Aluminium sheets between which O-M was sandwiched, as well as compression/sealing force. Therefore, one interesting future research topic is to systematically investigate the key parameters for fabricating membranes with smooth surface. Besides, it is obvious that the surface of F-M was also not smooth (shown in the first column of Figure 4) due to rough surface of S-M.

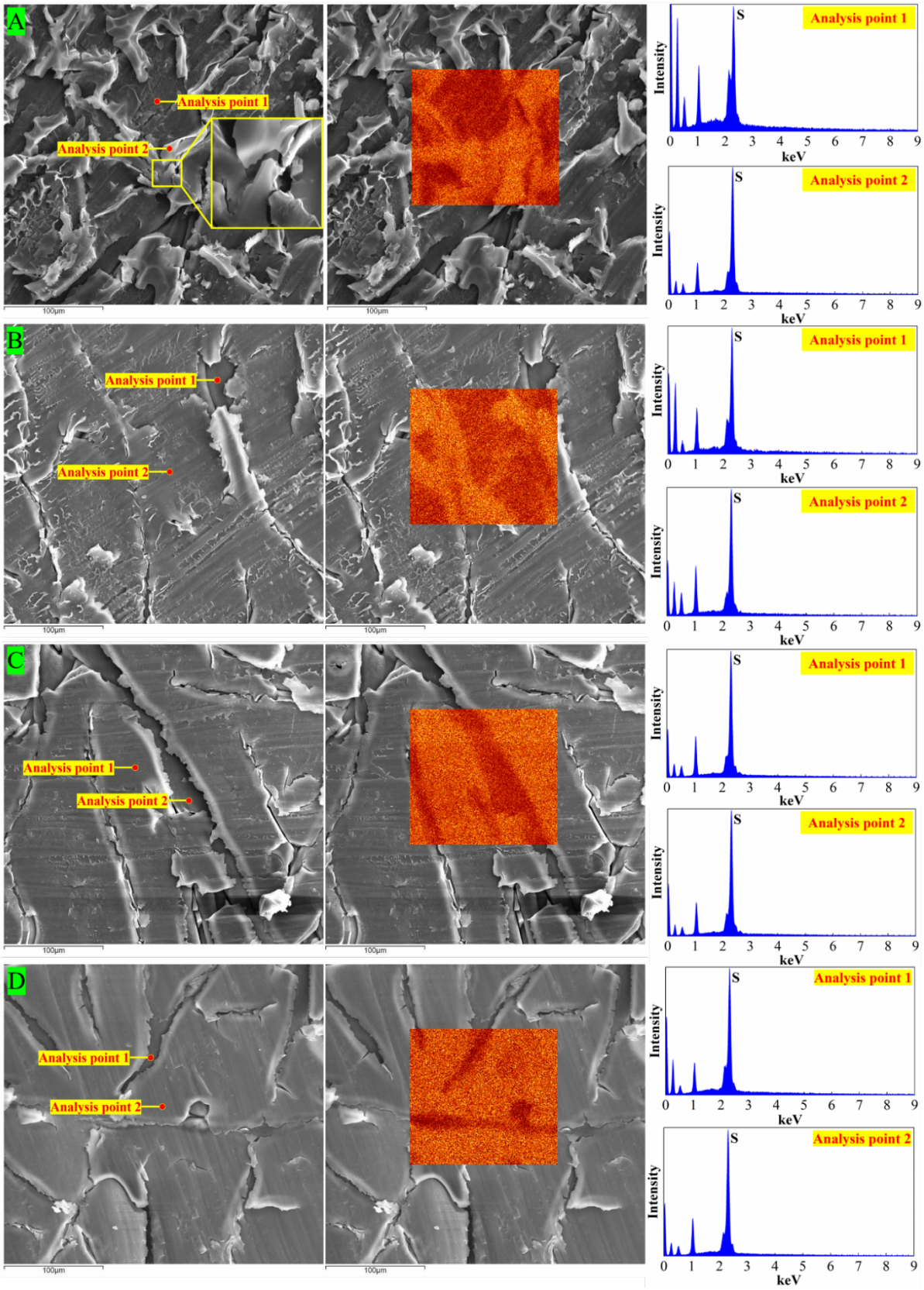


Figure 4. Surface morphology, sulfur mapping and energy spectrum diagram of F-M with different sulfonation reaction time. (A) F-M-22 (B) F-M-30 (C) F-M-38 (D) F-M-46. The number following F-M means sulfonation hours.

Sulfur mapping technique was applied to investigate the distribution of functional groups (i.e., $-SO_3^-$) in the synthesized membranes. As revealed by the second column of Figure 4, the presence of sulfur on membrane surface was confirmed. The presence of sulfonate group was further confirmed by FTIR technique. Also, it is interesting to point out that the appearance of sulfur mapping was consistent with the uneven membrane surface. This is actually one limitation of elemental mapping technique. In other words, membrane surface topography could have an important effect on EDX signals. Therefore, it does not necessarily mean that sulfur was less abundant in relatively darker area of the mapping. A further analysis method was applied to gain a better understanding of the presence of sulfonate groups on membrane surface. Two typical points were selected on each membrane and their energy spectrum diagrams were obtained. As shown in the third column of Figure 4, both energy spectrum diagrams in all membranes shown high sulfur peaks. In brief, combing sulfur mapping and energy spectrum diagram, sulfur was successfully introduced to membrane surface. Besides, in order to investigate whether sulfonation reaction also took place across the membrane, two typical points across the membrane samples were selected and their energy spectrum diagrams were analyzed. As shown in Figure 5, sulfur peaks were observed in energy spectrum diagrams of all the membranes. Therefore, it was safe to conclude that sulfonation reaction took place both on membrane surface and across the membrane.

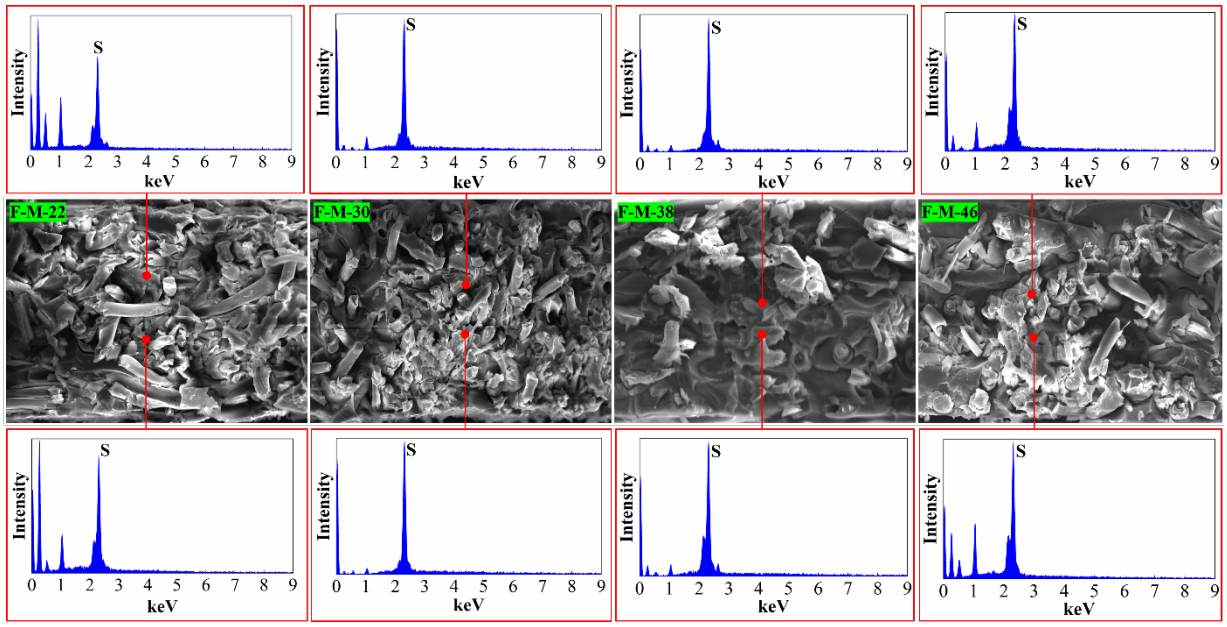


Figure 5. Energy spectrum diagram of F-M cross-sections.

3.2. Membrane chemical structure

The chemical structure of O-M, S-M and F-M were revealed by FTIR spectra (Figure 6). Polypropylene as O-M composition was verified by FTIR spectrum.[36–38] The most prominent peaks were observed at around 2915 cm^{-1} and 2849 cm^{-1}, corresponding to asymmetrical and symmetrical CH_2 stretching vibration, respectively. The peaks at 1462 cm^{-1} and 1473 cm^{-1} were attributed to asymmetrical CH_3 bending vibration while the peak at 1376 cm^{-1} was

corresponding to symmetrical CH_3 bending vibration. The next remarkable peaks at 718 cm^{-1} and 732 cm^{-1} were owing to CH_2 wagging vibration.

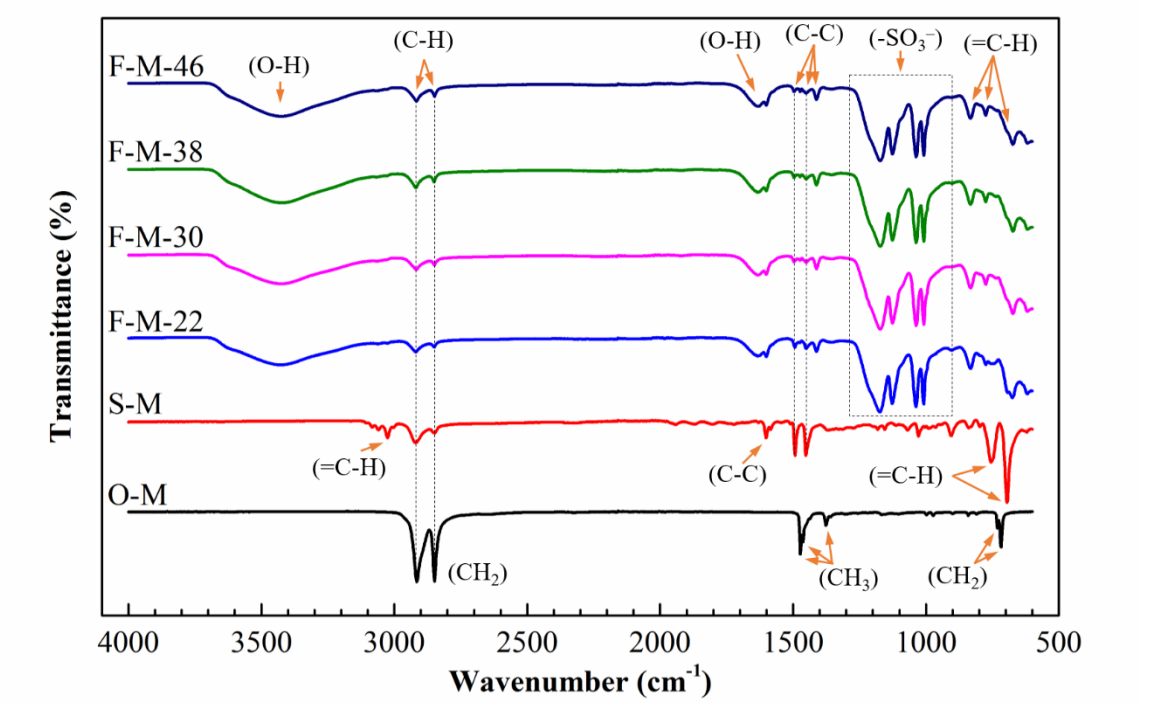


Figure 6. FTIR spectra of O-M, S-M and F-M. O-M referred to the original PP membrane support; S-M referred to the semi-finished membrane synthesized by copolymerization of St and DVB in O-M; F-M referred to the final-membrane synthesized by sulfonation of S-M. The number following F-M means sulfonation hours.

For S-M spectrum, the first prominent peak at 3025 cm^{-1} was due to aromatic =C-H stretching vibration, the peaks at 2920 cm^{-1} and 2849 cm^{-1} were due to alkyl C-H stretching vibrations, the next peaks at 1601 cm^{-1}, 1493 cm^{-1}, and 1451 cm^{-1} were due to aromatic -C=C- bond stretching vibration, and the peaks at 755 cm^{-1} and 695 cm^{-1} indicated aromatic =C-H bending vibration.[39] In short, S-M spectrum revealed that polystyrene was successfully formed in membrane support. For F-M spectrum, the most remarkable peaks for confirming sulfonation of polystyrene were observed at 1174 cm^{-1}, 1127 cm^{-1}, 1038 cm^{-1} and 1009 cm^{-1}, where the first two peaks were corresponding to asymmetric stretching vibration of sulfonate group while the latter two peaks were attributed to symmetric stretching vibration of sulfonate group.[39,40] Besides, the range 3000 – 3700 cm^{-1} was due to stretching vibration of H_2O, the peaks at 2920 cm^{-1} and 2849 cm^{-1} were due to alkyl C-H stretching vibrations, the peak at 1634 cm^{-1} was due to O-H bending vibration of H_2O, the weak peaks at 1496 cm^{-1}, 1451 cm^{-1} and 1412 cm^{-1} corresponded to aromatic -C=C- bond stretching vibration, the peaks at 832 cm^{-1},775 cm^{-1} and 673 cm^{-1} were due to aromatic =C-H out of plane bending vibration, and the peak at 618 cm^{-1} was due to ring in-plane bending vibration.[41–44] In a nutshell, F-M spectra demonstrated that functional sulfonate groups were successfully introduced to F-M through functionalization of polymers. Furthermore, FTIR spectrum of S-M indicated that polypropylene support fabric was fully covered by polystyrene. These results corresponded

well with membrane surface morphology and sulfur distribution discussed above.

3.3. Ion exchange capacity

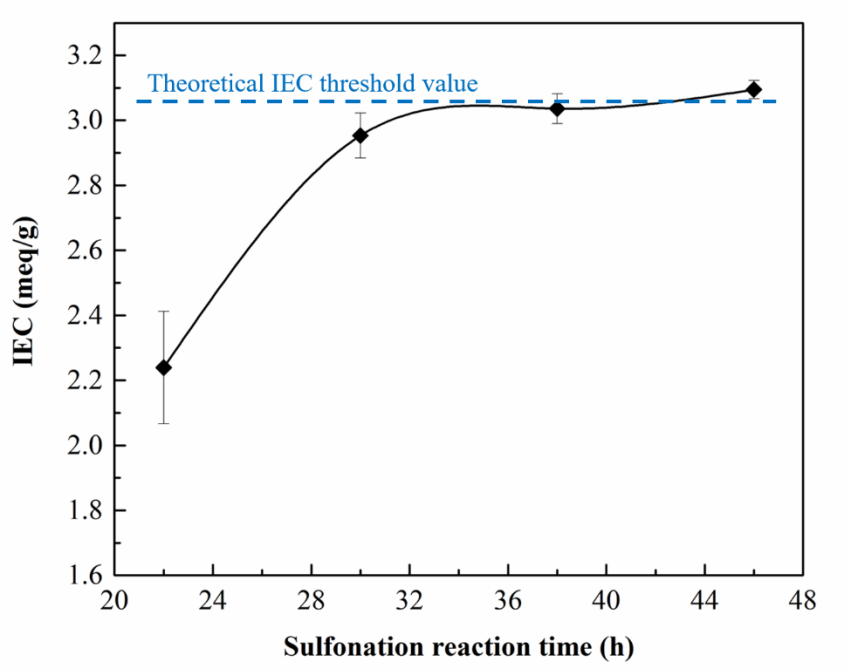
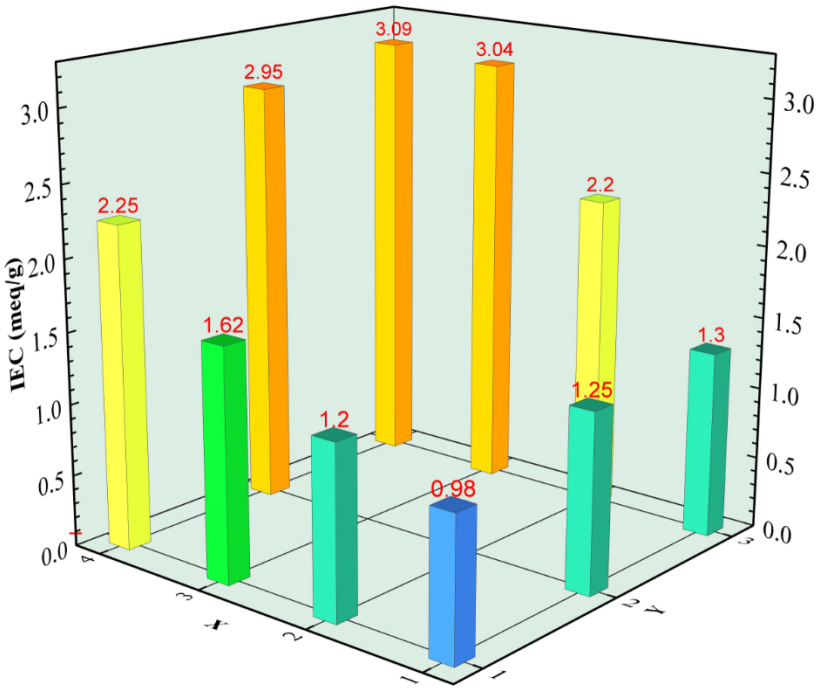


Figure 7. Effect of sulfonation reaction time on IEC. Values are averages of at least three replicates. Error bars represent one standard deviation.

As shown in Figure 7, all the synthesized membranes showed high IEC. IEC of the synthesized membranes (F-M-30, F-M-38 and F-M-46) were compared with common commercial cation exchange membranes (Figure 8).[45,46] As revealed by Figure 8, our synthesized membranes demonstrated excellent IEC performance compared with other membranes. The high IEC was mainly due to high mas ratio of polystyrene to polypropylene in S-M, which could reach around 1:1 based on experiment results. The high IEC was also indicated by sulfur distribution as well as FTIR analysis discussed above. Furthermore, IEC increased with increasing sulfonation reaction time, but reached a threshold value (~3mmol/g), which was consistent with theoretical IEC threshold value (see Supporting Information for details). One significant point of this agreement lied in that it provided a straightforward way to design membranes with different IEC using this novel methodology. In other words, the IEC of membranes could be designed to meet different requirements simply by controlling the mass ratio of functional polymers to membrane support as well as the sulfonation reaction time. And the IEC (threshold value) could be predicted by theoretical calculation without carrying out extensive experiments.



(X,Y)	Membrane	(X,Y)	Membrane	(X,Y)	Membrane
(4,3)	F-M-46	(3,3)	F-M-38	(1,3)	Fumasep® FKD
(4,2)	F-M-30	(3,1)	Neosepta® CMX	(1,2)	Fumasep® FKB
(4,1)	Neosepta® CM-1	(2,3)	Ralex® CMH-PES	(1,1)	Nafion™ N117
/	/	(2,1)	Chemjoy® CJMCED	/	/

Figure 8. Comparison of IEC between prepared membranes in this study and common commercial membranes.

3.4. Water contact angle, water uptake and conductivity

Water contact angle of O-M decreased quickly and changed from A (1) to A (4) in less than 10 seconds, indicating the porous structure of O-M (Figure 9A). S-M was hydrophobic due to the formation of crosslinked polystyrene (Figure 9B). When a water droplet was placed down on F-M, it spread very quickly and completely, and was much faster than O-M, and thus making it unable to observe the changes of contact angle shown in O-M (Figure 9C). In a nutshell, the water contact angles of membranes experienced fluctuating changes at different fabricating stages (Figure 9D), indicating the successful reactions of polymerization and sulfonation. It is important to point out that F-M demonstrated super hydrophilic property. Also, as revealed by Table 1, these membranes showed high water uptake. However, it should be pointed out that although these two properties could play a positive role in reducing membrane resistance, super hydrophilic property and high water uptake could have a negative impact on membrane dimensional stability since they had a positive relationship with membrane swelling. In other words, they could have some passive effect on desalination as water diffusion across the membranes could more easily took place. The issue of water diffusion could be solved by reducing sulfonation reaction time (see section 4 and 5 in Supporting Information for more details). However, a disadvantage of this method was that reducing sulfonation reaction time could also reduce the efficiency of ED due to high membrane resistance. Therefore, future

research should aim to reduce membrane water uptake and hydrophilicity while maintaining their high IEC performance. One strategy adopted by researchers to reduce water uptake of ion exchange membranes was through incorporation of phase separation in the membranes.[13]

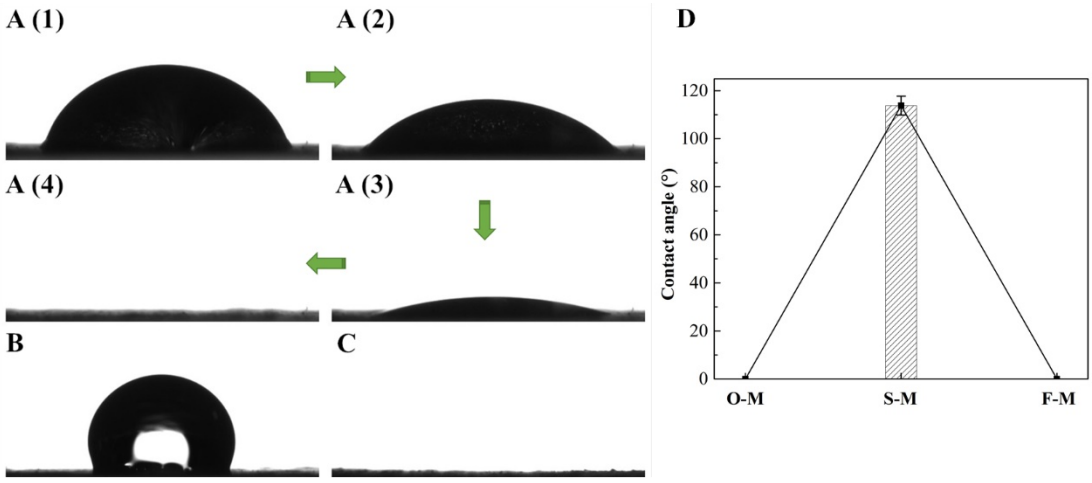


Figure 9. Measurement of the water contact angle of (A) original PP membrane support (O-M), (B) semi-finished membrane (S-M), and (C) final-membrane (F-M). Comparison of water contact angles of membranes at different stages is shown in (D). Values are averages of at least three replicates. Error bars represent one standard deviation.

As indicated by Table 1, the conductivity of membranes showed a tendency to increase with increasing sulfonation reaction time, indicating the positive relationship between conductivity and IEC.

Table 1. Water uptake and conductivity of synthesized CEMs

Membrane	Water uptake (%)	Conductivity (mS/cm)
F-M-22	72.5 ± 1.4	22.37 ± 1.43
F-M-30	101.7 ± 10.9	24.93 ± 0.66
F-M-38	94.1 ± 8.2	29.04 ± 0.36
F-M-46	92.9 ± 5.1	30.39 ± 0.56

Note: the conductivity values given in Table 1 correspond to proton conductivity.

3.5. Membrane thermal properties

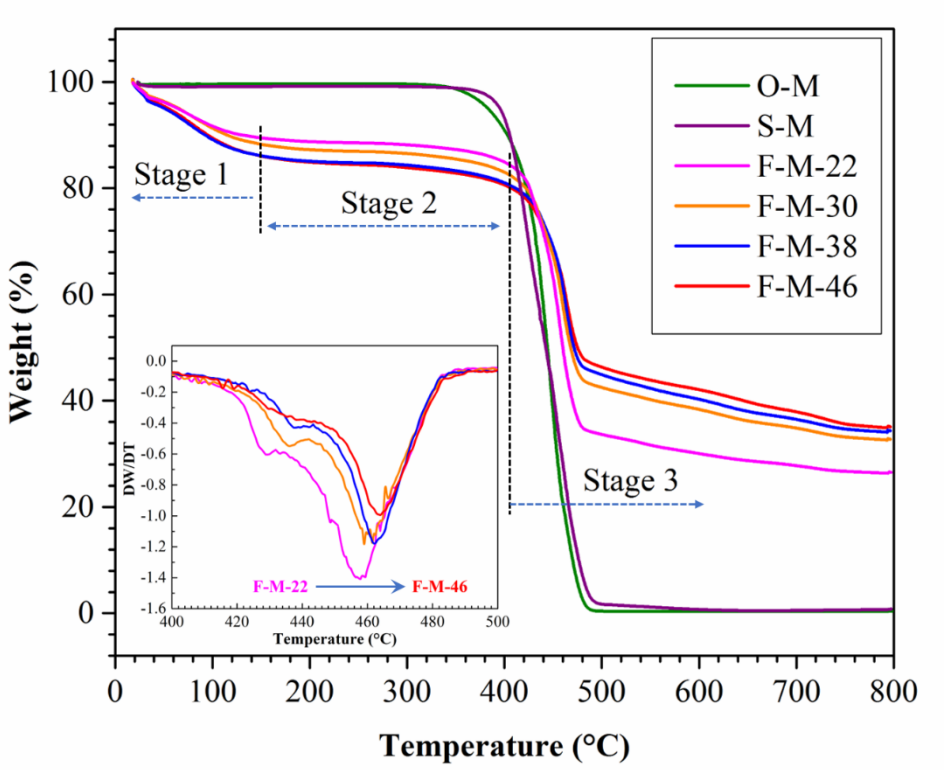


Figure 10. TGA diagrams of original PP membrane support (O-M), semi-finished membrane (S-M), and final-membrane (F-M) with different sulfonation reaction time. The number following F-M means sulfonation hours.

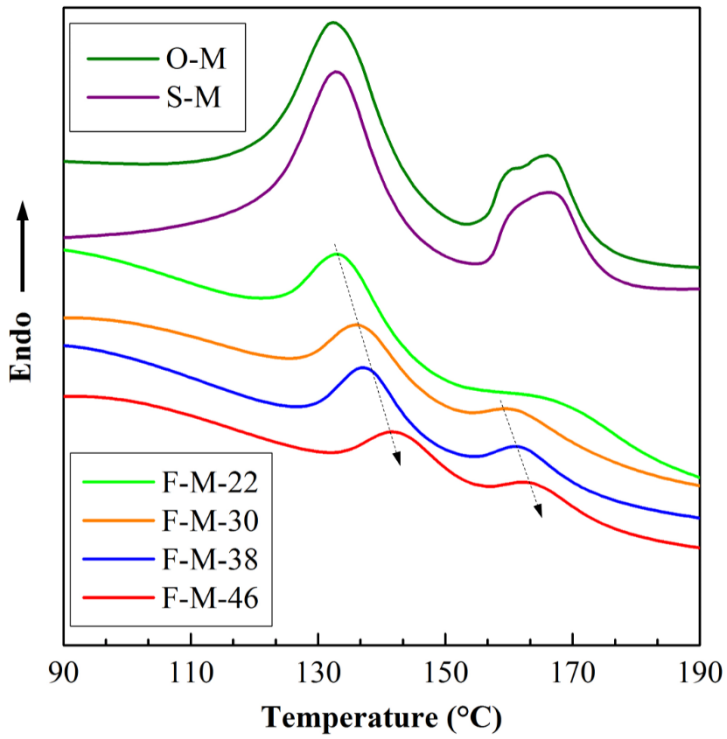


Figure 11. DSC diagrams of original PP membrane support (O-M), semi-finished membrane (S-M), and final-membrane (F-M) with different sulfonation reaction time. The number following F-M means sulfonation hours.

As shown in Figure 10, O-M and S-M demonstrated excellent thermo-stable property which did not decompose until at high temperature (> 300 °C). For F-M, there were three stages of weight loss as temperature was increased, including the loss of absorbed water (i.e., dehydration stage), followed by thermal decomposition of sulfonate group (i.e., desulfonation stage), and finally degradation of polymer chains (i.e., carbonization stage). The presence of hydrate water was also indicated by FTIR spectra as discussed above. Besides, TGA results revealed that a significant mass fraction of F-M remained at about 800 °C, which was different from O-M and S-M whose weight percent already reached zero at about 500 °C indicating no residues or negligible residues left. This was most likely a result of the formation of a highly heat-resistant sulfur-bridged (e.g., -SO_2-) polymer during pyrolysis.[47,48] Furthermore, the mass fraction of F-M residues showed a trend to increase with increasing sulfonation reaction time, with F-M-22 having the lowest ratio of residues while F-M-46 having the highest ratio of residues. TGA results also revealed that F-M-22 had the lowest ratio of water content while F-M-38 and F-M-46 showed the highest ratio of water content. These results indicated that the amount of functional sulfonate groups in F-M tended to increase with increasing sulfonation reaction time. This agreed well with the results revealed by other characterization techniques discussed above. Additionally, in the derivative weight loss curves of F-M in the range of 400 to 500 °C, the maximum degradation rate tended to shift to higher temperatures with increasing sulfonation reaction time. Also, as revealed by DSC curves (Figure 11), O-M showed multiple melting peaks (two obvious peaks and one less obvious peak) and the melting peaks for F-M tended to shift to higher temperatures with increasing sulfonation reaction time (see Table S1 in Supporting Information for details). These results might indicate that thermal stability of F-M was slightly improved with increasing sulfonation reaction time. Given the modest operating temperature for desalination using electrodialysis, F-M demonstrated sufficient thermal stability to meet the requirements, which was comparable to many other kinds of cation exchange membranes.[16,18,49]

4. CONCLUSIONS

In this work, we proposed a novel methodology for making high ion-exchange capacity cation exchange membranes using porous polypropylene as membrane support and sulfonated polystyrene as functional polymers. The polymerization and sulfonation reactions successfully took place in membrane support. The synthesized membranes demonstrated superior IEC (up to 3mmol/g), attributing to high amount of functional polymers introduced in the synthesized membranes. Especially, theoretical IEC threshold value corresponded well with experimental threshold value, indicating that IEC could be specifically designed without carrying out extensive experiments. Further, sulfonate groups were distributed both on membrane surface and across the membranes, which agreed well with high IEC of synthesized membranes. Besides, the semi-finished membrane demonstrated hydrophobic property due to formation of polystyrene. By comparison, the final membranes showed super hydrophilic property as well as high water uptake. In addition, when sulfonation reaction time increased, the conductivity of membranes also showed a tendency to increase, revealing the positive relationship between conductivity and IEC. Finally, the final membranes showed sufficient thermal stability for

electrodialysis applications such as water desalination. This novel methodology may open up new possibilities for fabricating ion exchange membranes with superior ion exchange capacity. Future research work will be to study the effectiveness of this novel methodology for other materials for cation exchange membranes as well as anion exchange membranes. Furthermore, future research should aim to reduce membrane water uptake and hydrophilicity while maintaining their high IEC performance.

ASSOCIATED CONTENT

Supporting Information
Theoretical IEC threshold value; conductivity measurement and calculation; melting temperatures of O-M, S-M and F-M; mass production of membranes; electrodialysis system and tests

AUTHOR INFORMATION

Corresponding Author
*Email: b.ladewig@imperial.ac.uk

ORCID
Bradley P. Ladewig: 0000-0002-2135-1913
Shanxue Jiang: 0000-0002-3859-3345

Notes
The authors declare no competing financial interest.

ACKNOWLEDGMENTS

B. P. Ladewig gratefully acknowledge financial support from Imperial College London. S. Jiang gratefully acknowledge Department of Chemical Engineering at Imperial College London for providing the PhD scholarship. The authors would like to thank David Crawford for his significant efforts in building up the electrodialysis system. We thank Dr. Bo Wang for his help during the water contact angle measurement process. We thank Patricia Carry for her help with the PerkinElmer ICP instrument.

REFERENCES

(1) Cassady, H. J.; Cimino, E. C.; Kumar, M.; Hickner, M. A. Specific Ion Effects on the Permselectivity of Sulfonated Poly(ether Sulfone) Cation Exchange Membranes. *J. Memb. Sci.* **2016**, *508*, 146–152.
(2) Ge, L.; Wu, L.; Wu, B.; Wang, G.; Xu, T. Preparation of Monovalent Cation Selective Membranes through Annealing Treatment. *J. Memb. Sci.* **2014**, *459*, 217–222.
(3) Vaselbehagh, M.; Karkhanechi, H.; Takagi, R.; Matsuyama, H. Biofouling Phenomena

on Anion Exchange Membranes Under the Reverse Electrodialysis Process. *J. Memb. Sci.* **2017**, *530* (November 2016), 232–239.

(4) Kim, D. H.; Park, H. S.; Seo, S. J.; Park, J. S.; Moon, S. H.; Choi, Y. W.; Jiong, Y. S.; Kim, D. H.; Kang, M. S. Facile Surface Modification of Anion-Exchange Membranes for Improvement of Diffusion Dialysis Performance. *J. Colloid Interface Sci.* **2014**, *416*, 19–24.

(5) Park, C. H.; Lee, S. Y.; Hwang, D. S.; Shin, D. W.; Cho, D. H.; Lee, K. H.; Kim, T.-W.; Kim, T.-W.; Lee, M.; Kim, D.-S.; Doherty, C. M.; Thornton, A. W.; Hill, A. J.; Guiver, M. D.; Lee, Y. M. Nanocrack-Regulated Self-Humidifying Membranes. *Nature* **2016**, *532* (7600), 480–483.

(6) Lee, J. H.; Lee, J. Y.; Kim, J. H.; Joo, J.; Maurya, S.; Choun, M.; Lee, J.; Moon, S. H. SPPO Pore-Filled Composite Membranes with Electrically Aligned Ion Channels via a Lab-Scale Continuous Caster for Fuel Cells: An Optimal DC Electric Field Strength-IEC Relationship. *J. Memb. Sci.* **2016**, *501*, 15–23.

(7) Li, Y.; Lin, X.; Wu, L.; Jiang, C.; Hossain, M. M.; Xu, T. Quaternized Membranes Bearing Zwitterionic Groups for Vanadium Redox Flow Battery through a Green Route. *J. Memb. Sci.* **2015**, *483*, 60–69.

(8) Tong, B.; Hossain, M. M.; Yang, Z.; Cheng, C.; Wang, Y.; Jiang, C.; Xu, T. Development of Heterogeneous Cation Exchange Membranes Using Functional Polymer Powders for Desalination Applications. *J. Taiwan Inst. Chem. Eng.* **2016**, *67*, 435–442.

(9) Vera, E.; Sandeaux, J.; Persin, F.; Pourcelly, G.; Dornier, M.; Ruales, J. Modeling of Clarified Tropical Fruit Juice Deacidification by Electrodialysis. *J. Memb. Sci.* **2009**, *326* (2), 472–483.

(10) Abdu, S.; Martí-Calatayud, M.-C.; Wong, J. E.; García-Gabaldón, M.; Wessling, M. Layer-by-Layer Modification of Cation Exchange Membranes Controls Ion Selectivity and Water Splitting. *ACS Appl. Mater. Interfaces* **2014**, *6*, 1843−1854.

(11) Abdu, S.; Sricharoen, K.; Wong, J. E.; Muljadi, E. S.; Melin, T.; Wessling, M. Catalytic Polyelectrolyte Multilayers at the Bipolar Membrane Interface. *ACS Appl. Mater. Interfaces* **2013**, *5* (21), 10445–10455.

(12) Allioux, F. M.; He, L.; She, F.; Hodgson, P. D.; Kong, L.; Dumée, L. F. Investigation of Hybrid Ion-Exchange Membranes Reinforced with Non-Woven Metal Meshes for Electro-Dialysis Applications. *Sep. Purif. Technol.* **2015**, *147*, 353–363.

(13) Chatterjee, U.; Bhadja, V.; Jewrajka, S. K. Effect of Phase Separation and Adsorbed Water on Power Consumption and Current Efficiency of Terpolymer Conetwork-Based Anion Exchange Membrane. *J. Mater. Chem. a* **2014**, *2* (38), 16124–16134.

(14) Chatterjee, U.; Jewrajka, S. K. Amphiphilic Poly(acrylonitrile)-Co-poly(2-Dimethylamino)ethyl Methacrylate Conetwork-Based Anion Exchange Membrane for Water Desalination. *J. Mater. Chem. A* **2014**, *2* (22), 8396–8406.

(15) Kristensen, M. B.; Haldrup, S.; Christensen, J. R.; Catalano, J.; Bentien, A. Sulfonated Poly(arylene Thioether Sulfone) Cation Exchange Membranes with Improved Permselectivity/ion Conductivity Trade-Off. *J. Memb. Sci.* **2016**, *520*, 731–739.

(16) Pandey, R. P.; Das, A. K.; Shahi, V. K. 2-Acrylamido-2-Methyl-1-Propanesulfonic Acid Grafted Poly(vinylidene Fluoride-Co-Hexafluoropropylene)-Based

Acid-/Oxidative-Resistant Cation Exchange for Membrane Electrolysis. *ACS Appl. Mater. Interfaces* **2015**, *7* (51), 28524–28533.

(17) Shukla, G.; Pandey, R. P.; Shahi, V. K. Temperature Resistant Phosphorylated Graphene Oxide-Sulphonated Polyimide Composite Cation Exchange Membrane for Water Desalination with Improved Performance. *J. Memb. Sci.* **2016**, *520*, 972–982.

(18) Khan, A. A.; Ahmad, R.; Zeeshan, M.; Shaheen, S. Synthesis, Characterization, Electrical and Dielectrical Studies of Polypyrrole-Sn(IV)arsenotungstate Nanocomposite Ion-Exchange Membrane: Its Selectivity as Ba(II). *J. Mol. Liq.* **2016**, *221*, 999–1007.

(19) Moghbeli, M. R.; Khajeh, A.; Alikhani, M. Nanosilica Reinforced Ion-Exchange polyHIPE Type Membrane for Removal of Nickel Ions: Preparation, Characterization and Adsorption Studies. *Chem. Eng. J.* **2017**, *309*, 552–562.

(20) White, N.; Misovich, M.; Yaroshchuk, A.; Bruening, M. L. Coating of Nafion Membranes with Polyelectrolyte Multilayers to Achieve High Monovalent/divalent Cation Electrodialysis Selectivities. *ACS Appl. Mater. Interfaces* **2015**, *7* (12), 6620–6628.

(21) Kamcev, J.; Paul, D. R.; Freeman, B. D. Effect of Fixed Charge Group Concentration on Equilibrium Ion Sorption in Ion Exchange Membranes. *J. Mater. Chem. A* **2017**, *5*, 4638–4650.

(22) Seo, J.; Kushner, D. I.; Hickner, M. A. 3D Printing of Micropatterned Anion Exchange Membranes. *ACS Appl. Mater. Interfaces* **2016**, *8* (26), 16656–16663.

(23) Ponce-Gonzalez, J.; Whelligan, D. K.; Wang, L.; SOUALHI, R.; Wang, Y.; Peng, Y.; Peng, H.; Apperley, D. C.; Sarode, H. N.; Pandey, T. P.; Divekar, A. G.; Seifert, S.; Herring, A.; Zhuang, L.; Varcoe, J. R. High Performance Aliphatic-Heterocyclic Benzyl-Quaternary Ammonium Radiation-Grafted Anion-Exchange Membranes. *Energy Environ. Sci.* **2016**, *9*, 3724–3735.

(24) Fontananova, E.; Messana, D.; Tufa, R. A.; Nicotera, I.; Kosma, V.; Curcio, E.; van Baak, W.; Drioli, E.; Di Profio, G. Effect of Solution Concentration and Composition on the Electrochemical Properties of Ion Exchange Membranes for Energy Conversion. *J. Power Sources* **2017**, *340*, 282–293.

(25) Xu, W.; Zhao, Y.; Yuan, Z.; Li, X.; Zhang, H.; Vankelecom, I. F. J. Highly Stable Anion Exchange Membranes with Internal Cross-Linking Networks. *Adv. Funct. Mater.* **2015**, *25* (17), 2583–2589.

(26) Ge, Q.; Ran, J.; Miao, J.; Yang, Z.; Xu, T. Click Chemistry Finds Its Way in Constructing an Ionic Highway in Anion-Exchange Membrane. *ACS Appl. Mater. Interfaces* **2015**, *7* (51), 28545–28553.

(27) Zhang, B.; Hong, J. G.; Xie, S.; Xia, S.; Chen, Y. An Integrative Modeling and Experimental Study on the Ionic Resistance of Ion-Exchange Membranes. *J. Memb. Sci.* **2017**, *524* (August 2016), 362–369.

(28) Dutta, K.; Das, S.; Kundu, P. P. Partially Sulfonated Polyaniline Induced High Ion-Exchange Capacity and Selectivity of Nafion Membrane for Application in Direct Methanol Fuel Cells. *J. Memb. Sci.* **2014**, *473*, 94–101.

(29) Li, X.; Zhao, Y.; Feng, Z.; Xiang, X.; Wang, S.; Xie, X.; Ramani, V. K. Ring-Opening Metathesis Polymerization for the Preparation of Polynorbornene-Based Proton Exchange Membranes with High Proton Conductivity. *J. Memb. Sci.* **2017**, *528* (July

2016), 55–63.
(30) Morandi, C. G.; Peach, R.; Krieg, H. M.; Kerres, J. Novel Morpholinium-Functionalized Anion-Exchange PBI–polymer Blends. *J. Mater. Chem. A* **2015**, *3* (3), 1110–1120.
(31) Klaysom, C.; Ladewig, B. P.; Lu, G. Q. M.; Wang, L. Preparation and Characterization of Sulfonated Polyethersulfone for Cation-Exchange Membranes. *J. Memb. Sci.* **2011**, *368* (1–2), 48–53.
(32) Bodner, M.; Cermenek, B.; Rami, M.; Hacker, V. The Effect of Platinum Electrocatalyst on Membrane Degradation in Polymer Electrolyte Fuel Cells. *Membranes (Basel)*. **2015**, *5* (4), 888–902.
(33) Shi, S.; Dursch, T. J.; Blake, C.; Mukundan, R.; Borup, R. L.; Weber, A. Z.; Kusoglu, A. Impact of Hygrothermal Aging on Structure/function Relationship of Perfluorosulfonic-Acid Membrane. *J. Polym. Sci. Part B Polym. Phys.* **2016**, *54* (5), 570–581.
(34) Nam, S. E.; Kim, S. O.; Kang, Y.; Lee, J. W.; Lee, K. H. Preparation of Nafion/sulfonated Poly(phenylsilsesquioxane) Nanocomposite as High Temperature Proton Exchange Membranes. *J. Memb. Sci.* **2008**, *322* (2), 466–474.
(35) Ranacher, C.; Resel, R.; Moni, P.; Cermenek, B.; Hacker, V.; Coclite, A. M. Layered Nanostructures in Proton Conductive Polymers Obtained by Initiated Chemical Vapor Deposition. *Macromolecules* **2015**, *48* (17), 6177–6185.
(36) Morent, R.; De Geyter, N.; Leys, C.; Gengembre, L.; Payen, E. Comparison between XPS- And FTIR-Analysis of Plasma-Treated Polypropylene Film Surfaces. *Surf. Interface Anal.* **2008**, *40* (3–4), 597–600.
(37) Andreassen, E. *Infrared and Raman Spectroscopy of Polypropylene*; Karger-Kocsis, J., Ed.; Kluwer Publishers, Dordrecht, 1999.
(38) Urbaniak-domagala, W. *The Use of the Spectrometric Technique FTIR-ATR to Examine the Polymers Surface*; Farrukh, M. A., Ed.; InTech, 2012.
(39) Li, L.; Ma, R.; Iyi, N.; Ebina, Y.; Takada, K.; Sasaki, T. Hollow Nanoshell of Layered Double Hydroxide. *Chem. Commun. (Camb).* **2006**, *2* (29), 3125–3127.
(40) Orler, E. B.; Yontz, D. J.; Moore, R. B. Sulfonation of Syndiotactic Polystyrene for Model Semicrystalline Ionomer Investigations. *Macromolecules* **1993**, *26*, 5157–5160.
(41) Luo, J.; Chen, Y.; Ma, Q.; Liu, R.; Liu, X. Layer-by-Layer Self-Assembled Hybrid Multilayer Films Based on Poly(sodium 4-Styrenesulfonate) Stabilized Graphene with Polyaniline and Their Electrochemical Sensing Properties. *RSC Adv.* **2013**, *3* (39), 17866–17873.
(42) Wang, Y. .; Liu, K. . b; Luo, Z. .; Duan, Y. . Preparation and Tumor Cell Model Based Biobehavioral Evaluation of the Nanocarrier System Using Partially Reduced Graphene Oxide Functionalized by Surfactant. *Int. J. Nanomedicine* **2015**, *10*, 4605–4620.
(43) Brijmohan, S. B.; Swier, S.; Weiss, R. A.; Shaw, M. T. Synthesis and Characterization of Cross-Linked Sulfonated Polystyrene Nanoparticles. *Ind. Eng. Chem. Res.* **2005**, *44* (21), 8039–8045.
(44) Cho, W.; Im, S.; Kim, S.; Kim, S.; Kim, J. Synthesis and Characterization of PEDOT:P(SS-Co-VTMS) with Hydrophobic Properties and Excellent Thermal Stability. *Polymers (Basel).* **2016**, *8* (5), 189.
(45) Ran, J.; Wu, L.; He, Y.; Yang, Z.; Wang, Y.; Jiang, C.; Ge, L.; Bakangura, E.; Xu, T. Ion

Exchange Membranes: New Developments and Applications. *J. Memb. Sci.* **2017**, *522*, 267–291.

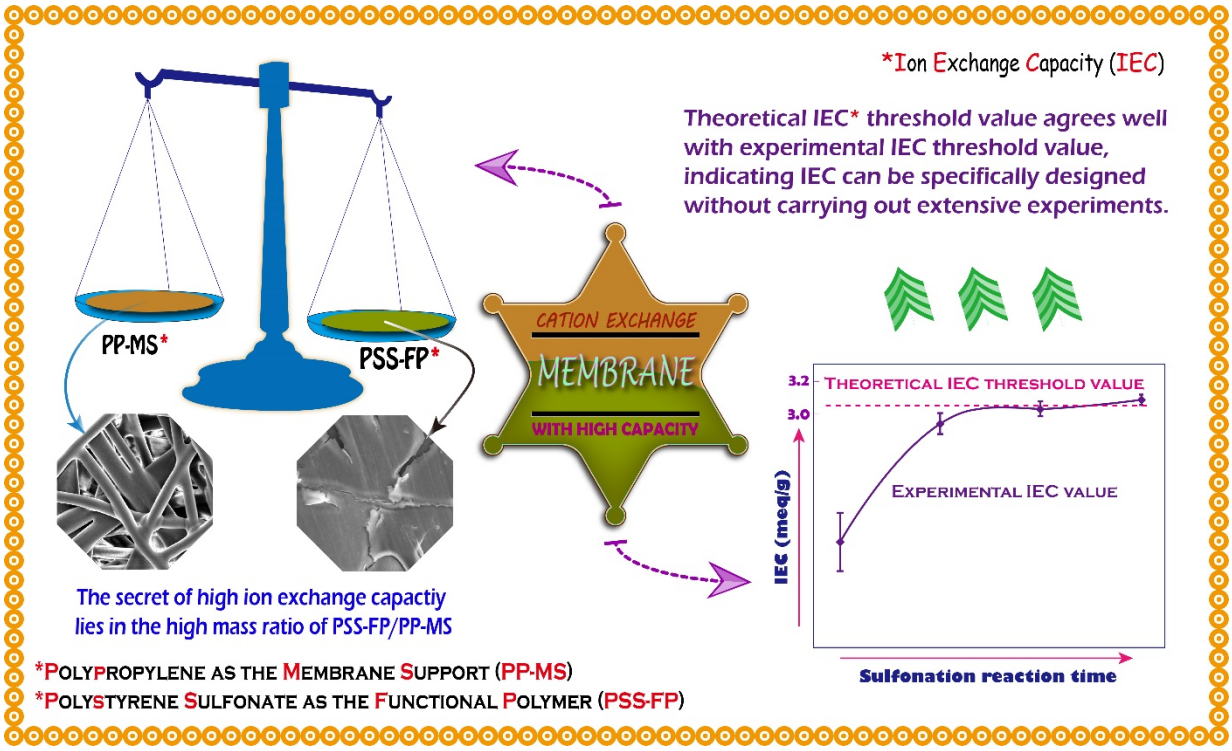
(46) Hosseini, S. M.; Gholami, A.; Koranian, P.; Nemati, M.; Madaeni, S. S.; Moghadassi, A. R. Electrochemical Characterization of Mixed Matrix Heterogeneous Cation Exchange Membrane Modified by Aluminum Oxide Nanoparticles: Mono/bivalent Ionic Transportation. *J. Taiwan Inst. Chem. Eng.* **2014**, *45* (4), 1241–1248.

(47) Neely, J. W. Characterization of Polymer Carbons Derived from Porous Sulfonated Polystyrene. *Carbon N. Y.* **1981**, *19* (1), 27–36.

(48) Matsuda, M.; Funabashi, K.; Yusa, H.; Kikuchi, M. Influence of Functional Sulfonic Acid Group on Pyrolysis Characteristics for Cation Exchange Resin. *J. Nucl. Sci. Technol.* **1987**, *24* (2), 124–128.

(49) Mondal, A. N.; Dai, C.; Pan, J.; Zheng, C.; Hossain, M. M.; Khan, M. I.; Wu, L.; Xu, T. Novel Pendant Benzene Disulfonic Acid Blended SPPO Membranes for Alkali Recovery: Fabrication and Properties. *ACS Appl. Mater. Interfaces* **2015**, *7* (29), 15944–15954.

TABLE OF CONTENTS GRAPHIC



Supporting Information

High ion-exchange capacity semi-homogeneous cation exchange membranes prepared via a novel polymerization and sulfonation approach in porous polypropylene

Shanxue Jiang,[†] Bradley P. Ladewig[*,†]

[†]Barrer Centre, Department of Chemical Engineering, Imperial College London, United Kingdom

*Corresponding author: Bradley P. Ladewig b.ladewig@imperial.ac.uk

Contents

1. Theoretical IEC threshold value 2

2. Conductivity measurement and calculation 4

3. Melting temperatures of O-M, S-M and F-M 7

4. Mass production of membranes 8

5. Electrodialysis system and tests 11

References 20

1. Theoretical IEC threshold value

Below are the terminologies used in the process of calculating theoretical IEC threshold value.

- IEC_{thr}: theoretical IEC threshold value
- IEC_{max}: maximum IEC that a membrane/resin can achieve in theory
- MW_{SO3H}: molecular weight of $-SO_3H$ group, i.e., 81 g/mol
- $MW_{Styrene}$: molecular weight of styrene, i.e., 104 g/mol
- PSS: polystyrene sulfonate
- W_{PP}: weight of polypropylene membrane support
- W_{PS}: weight of polystyrene formed in polypropylene membrane support
- W_{PSS}: weight of polystyrene sulfonate formed in polypropylene membrane support
- W_S: weight of sulfonate formed in polypropylene membrane support
- $W_{semi\text{-}mem}$: weight of semi-membrane synthesized by copolymerization of styrene and divinylbenzene in polypropylene membrane support
- $W_{final\text{-}mem}$: weight of final-membrane synthesized by sulfonation of semi-membrane via concentrated sulfuric acid
- p: practice coefficient
- r: mass ratio of polystyrene to polypropylene in semi-membrane
- m: mass fraction of polystyrene sulfonate in final-membrane

The relationship between different parameters is summarized as follows.

- $W_{semi\text{-}mem} = W_{PP} + W_{PS}$
- $W_{final\text{-}mem} = W_{PP} + W_{PSS}$
- $W_{PSS} = W_{PS} + W_S$
- $W_S = W_{PS} * MW_{SO3H}/MW_{Styrene}$ (Note: this relationship is based on the assumption that the weight loss of H during sulfonation is negligible, and the effect of DVB is not considered. Instead, its effect is reflected by practice coefficient)
- $IEC_{max} = 1000/(MW_{SO3H} + MW_{Styrene} - 1)$
- $r = W_{PS}/W_{PP}$
- $m = W_{PSS}/W_{final\text{-}mem}$
- $IEC_{thr} = p*m*IEC_{max}$

For PSS based cation exchange membrane/resin, the IEC_{max} that the membrane/resin could achieve theoretically is around 5.43 mmol/g. The calculation process is:

- $IEC_{max} = 1000/(81 + 104 – 1) \approx 5.43$ mmol/g

But in practice it was very difficult to achieve this value due to different factors such as sulfonation degree, the effect of DVB, etc. Besides, the resin usually has higher IEC compared to membranes (by dry weight). This is mainly because that for membranes, membrane support is usually required to increase the thermal and mechanic reliability of the membranes, which has a negative effect on IEC. Therefore, for theoretical calculation, a practice coefficient p is applied. p is defined as the ratio of highest IEC of common commercial sulfonated polystyrene based cation exchange resins (mmol/g) to IEC_{max}. Since the highest IEC of common commercial PSS based cation exchange resins is around 4.8 mmol/g, the value of p can then be calculated. The calculation process is:

- $p = 4.8/5.43 \approx 0.88$

The value of r is around 1 based on experimental results. The value of m can then be calculated. The calculation process is:

- $m = W_{PSS}/W_{final\text{-}mem}$
  $= W_{PSS}/(W_{PP} + W_{PSS})$
  $= 1/(1 + W_{PP}/W_{PSS})$
  $= 1/[1 + W_{PP}/(W_{PS} + W_S)]$
  $= 1/[1 + 1/(W_{PS}/W_{PP} + W_S/W_{PP})]$
  $= 1/[1 + 1/(r + W_{PS}/W_{PP}*MW_{SO3H}/MW_{Styrene})]$
  $= 1/[1 + 1/(r + r*MW_{SO3H}/MW_{Styrene})]$
  $= 1/[1 + 1/(1 + 1*81/104)]$
  ≈ 0.64

Therefore, the theoretical IEC threshold value of the synthesized membranes in this study can be calculated. The calculation process is:

- $IEC_{thr} = 0.88*0.64*5.43 \approx 3.06$ mmol/g

2. Conductivity measurement and calculation

The parameters in equation (3), equation (4) as well Figure 3 of the manuscript had the following values. The distance between the inner electrodes was 0.5 cm, the width of hydrated membrane sample width was 0.5 cm, the thickness of hydrated membrane was 0.26 mm.

Nyquist plots were obtained from measurements using the EIS function of the potentiostat. Nyquist plots were used to calculate the impedance or resistance. A detailed instruction on using Nyquist plots to obtain membrane resistance could be found elsewhere.[1–3] Below were examples of Nyquist plots for all the conductivity experiments in this study. At least four repeated measurements were carried out for each membrane sample.

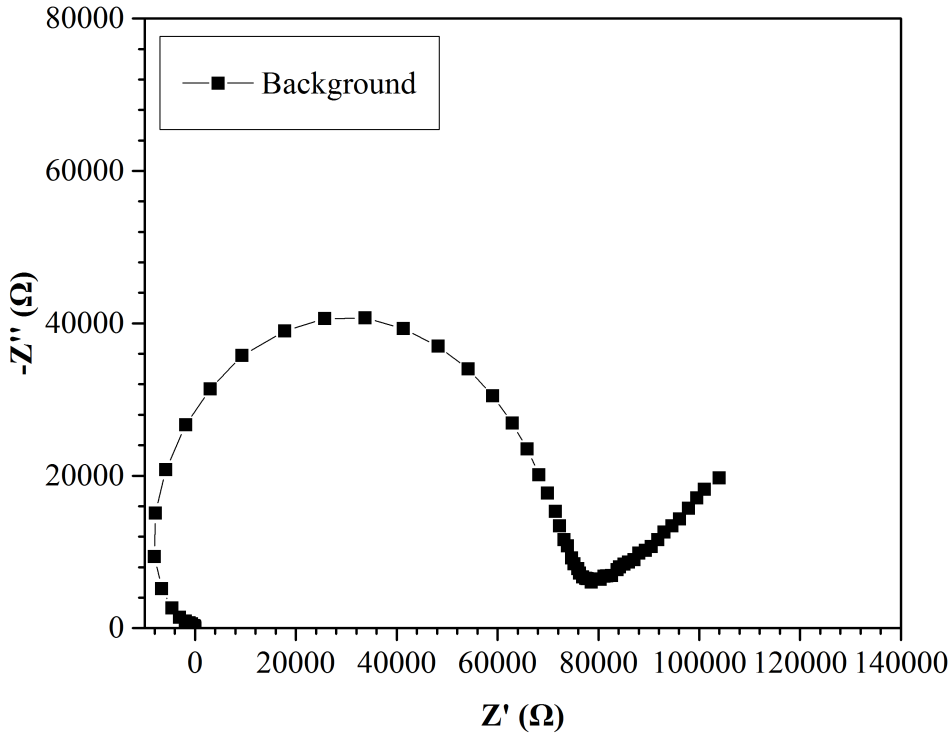


Figure S1. Nyquist plot obtained by AC impedance spectroscopy without membranes (Background). Z'' referred to imaginary impedance and Z' referred to real impedance.

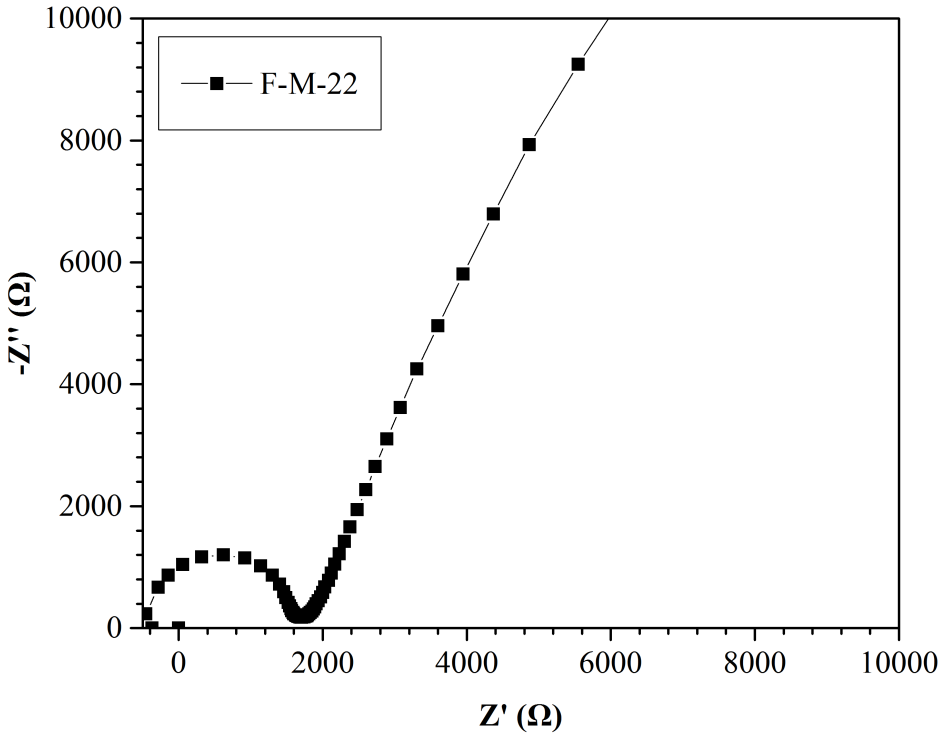


Figure S2. Nyquist plot obtained by AC impedance spectroscopy for membrane F-M-22. Z″ referred to imaginary impedance and Z′ referred to real impedance.

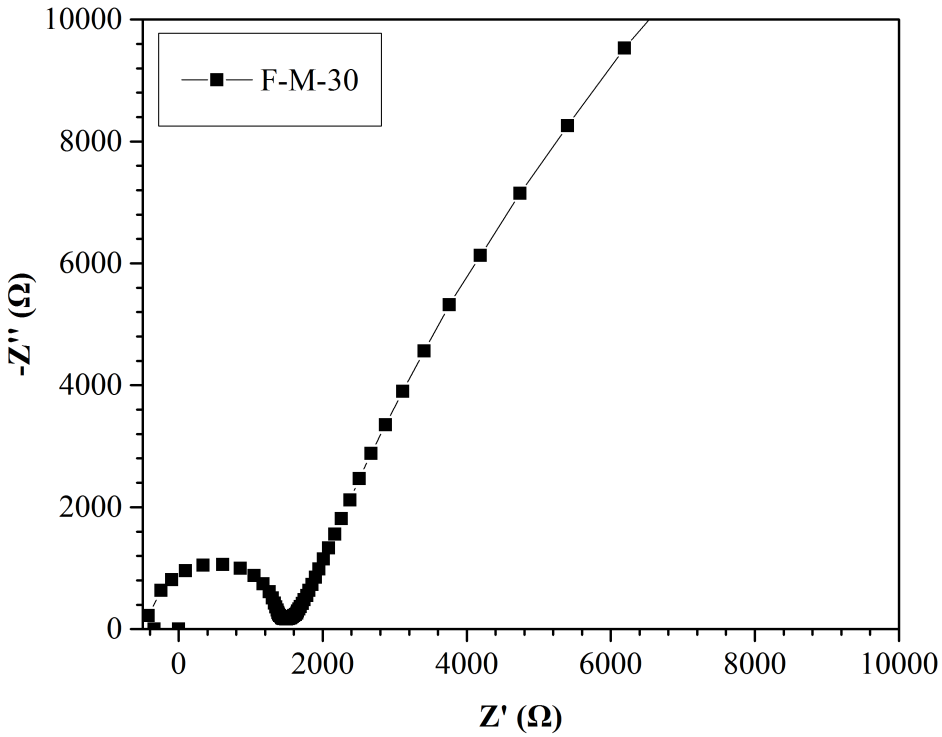


Figure S3. Nyquist plot obtained by AC impedance spectroscopy for membrane F-M-30. Z″ referred to imaginary impedance and Z′ referred to real impedance.

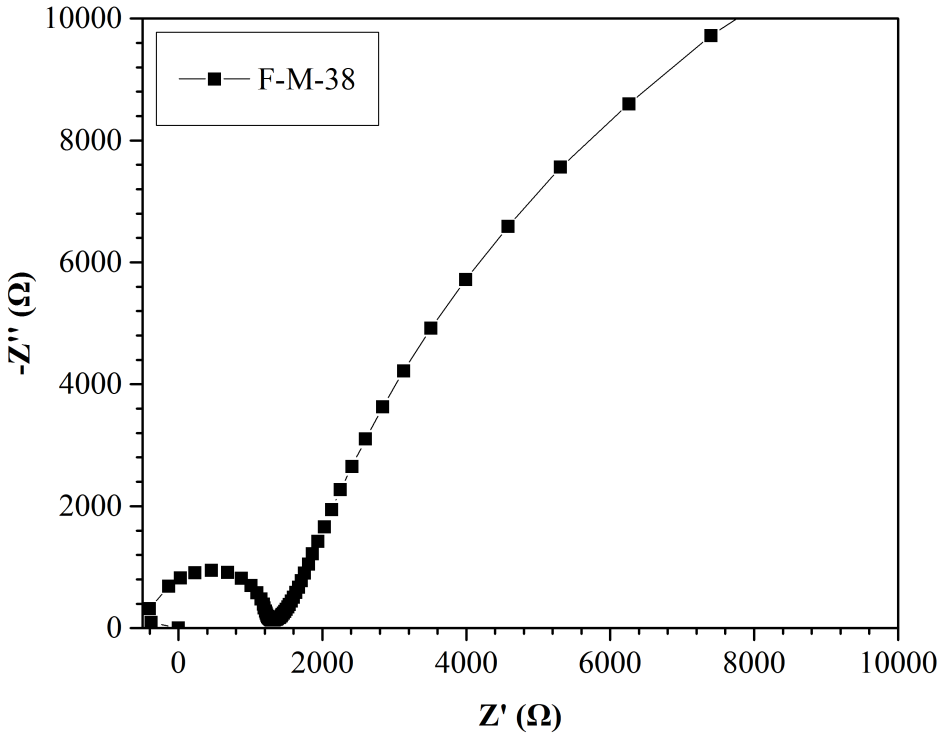


Figure S4. Nyquist plot obtained by AC impedance spectroscopy for membrane F-M-38. Z″ referred to imaginary impedance and Z′ referred to real impedance.

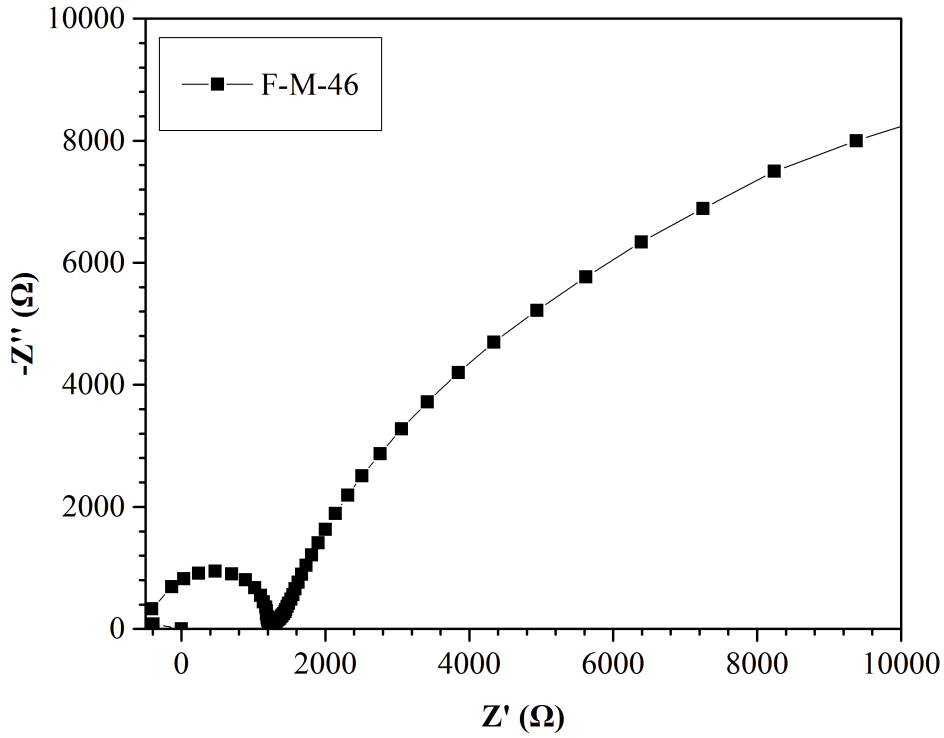


Figure S5. Nyquist plot obtained by AC impedance spectroscopy for membrane F-M-30. Z″ referred to imaginary impedance and Z′ referred to real impedance.

3. Melting temperatures of O-M, S-M and F-M

Table S1. Melting temperatures of O-M, S-M and F-M

Membrane	Melting temperature 1 (°C)	Melting temperature 2 (°C)
O-M	132.3	166.1
S-M	132.3	170.4
F-M-22	133.1	/
F-M-30	135.9	159.4
F-M-38	137.3	161.1
F-M-46	141.6	162.3

4. Mass production of membranes

The methodology introduced in this work could be used to produce many pieces of membranes at one time. In other words, it could be used for mass production of membranes, thus making it possible for industrial applications. The key thing was to find an effective spacer which should have very smooth surface and could not be dissolved by monomer solution. The spacer used in this study for demonstration of mass production of membranes was transparent polyester (PET) films which were kindly provided by HiFi Industrial Film. The PET film had a thickness of 125μm.

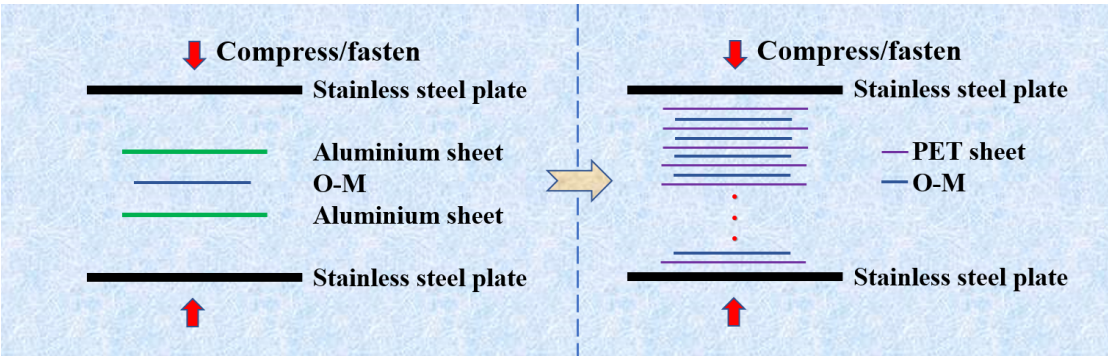


Figure S6. Methodology diagram for mass production of membranes. The left diagram was used in the manuscript where Aluminium sheet was the spacer. The right diagram showed mass production of membranes where original Aluminium sheet was replaced by PET sheet.

Figure S6 showed the methodology diagram for mass production of membranes. To be specific, the Aluminium sheet which was originally used as the spacer was replaced by PET sheet, and O-M containing monomer solution was separated by PET, one by one. Using this upgraded method, we can prepare many pieces of membranes at one time. Figure S7 showed the real pictures of our synthesized cation exchange membranes using the upgraded method. The six pieces of membranes were synthesized at one time rather than six times. The reason we synthesized six pieces lied in that it was the proper number of membranes used for further electrodialysis tests (section 5). It is undoubtedly feasible to prepare more pieces of membranes using this method if needed. Also, the membrane size was 11 cm × 11 cm, because the electrodialysis cell required this size of membranes (Figure S8). For industrial-scale production, much larger size membranes could be manufactured simply by enlarging the length of sides of stainless-

steel plates. The following equation could be used to estimate the volume of membranes produced at one time.

$$A = L*W*N$$

where A is the area of membranes (m^2), L and W are the length and width of O-M, respectively, and N is the number of O-M separated by PET films.

For example, if L = 1 m, W = 1 m, N =10, then A = 10 m^2, which means 10 m^2 membranes are synthesize at one time.

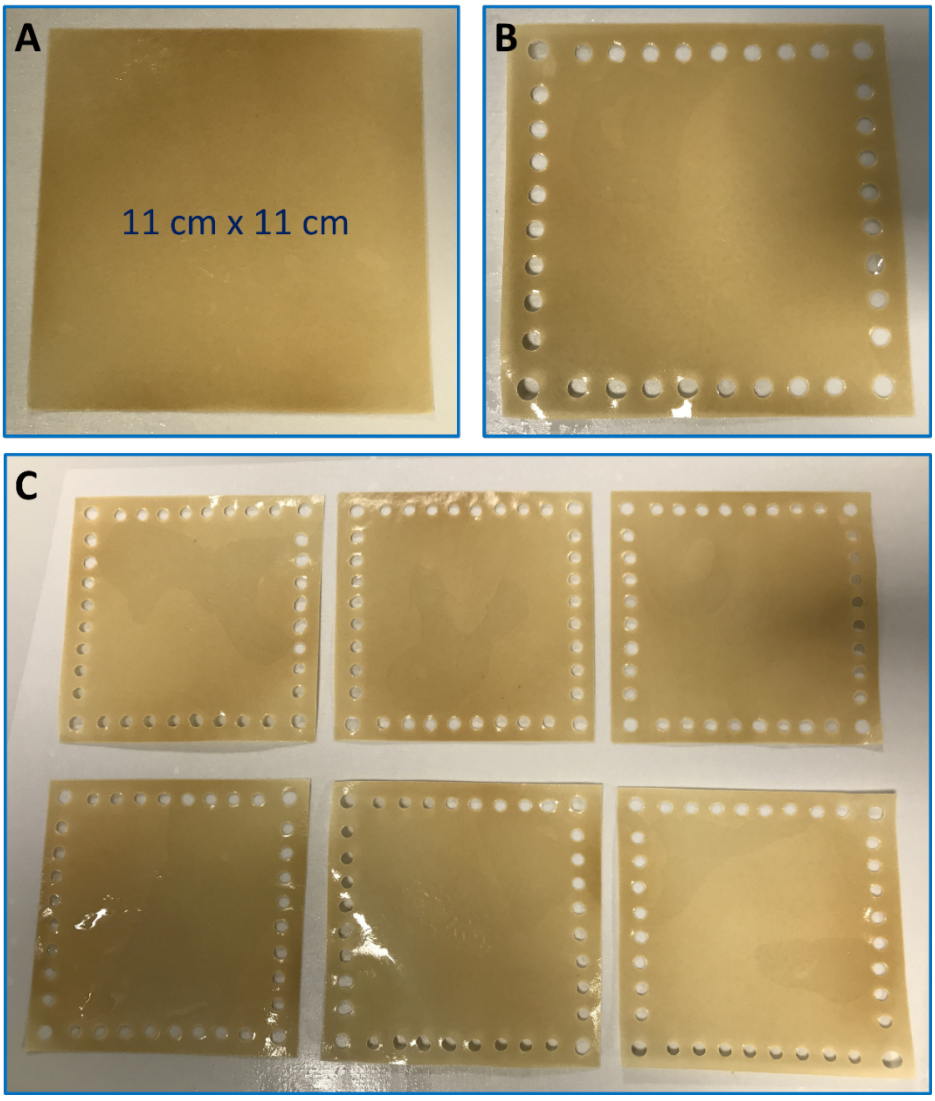


Figure S7. Real pictures of the synthesized cation exchange membranes for electrodialysis test. The sulfonation reaction time was 6 h. (A) Without holes. (B) With holes. The holes were channels for dilute and concentrate water. (C) Six pieces of membranes synthesized at one time.

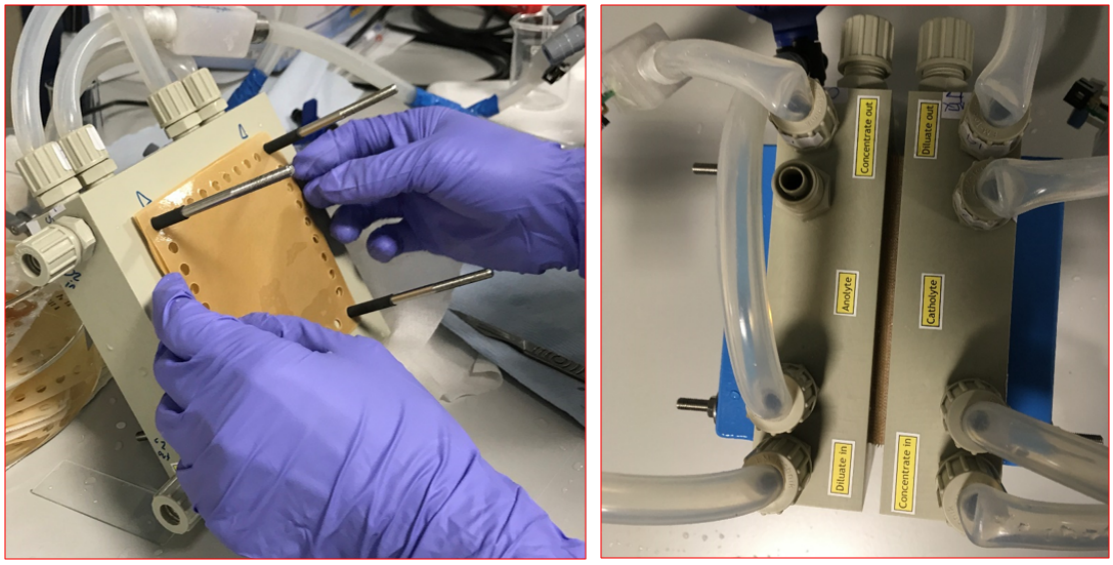


Figure S8. Real pictures of the electrodialysis cell with membranes.

Also, the synthesized membranes for electrodialysis test showed reduced water uptake (0.281±0.035) and water contact angle (Figure S9), indicating that these membranes were less hydrophilic compared to F-M-22, F-M-30, F-M-38 and F-M-46.

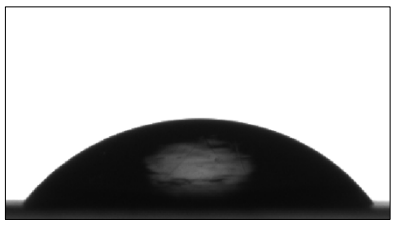


Figure S9. Water contact angle of the synthesized membranes for electrodialysis test.

5. Electrodialysis system and tests

5.1 Methods

Electrodialysis tests were conducted using an electrodialysis cell unit (model PCCell ED 64004) provided by PCCell GmbH, Germany. Cation exchange membranes (CEMs) used for electrodialysis tests were synthesized in this study while anion exchange membranes (AEMs) were purchased from PCA GmbH, Germany. Each of the ion exchange membrane had an active membrane area of 64 cm^2 (8 cm × 8 cm) as well as an effective size of 11 cm × 11cm. The membrane stack contained 5 cell pairs, which were composed of 6 cation exchange membranes, 5 anion exchange membranes, and 10 spacers. As shown by Figure S10, the system contained three compartments, namely dilute compartment, concentrate compartment and electrolyte (or electrode rinsing solution) compartment. The flow rates of these compartments were measured continuously in real time. An initial current was applied to the desalination system using a BioLogic VSP potentiostat and the current was recorded continuously in real time. The duration for the electrodialysis test was 60 minutes. Samples from the dilute compartment and concentrate compartment were collected at 0, 12, 24, 36, 48 and 60 min, respectively. The conductivity of these samples was measured using a TDS meter (model C100, Cole-Parmer, UK). Furthermore, the sodium concentration of these samples was measured using an inductively coupled plasma (ICP) instrument (Perkin-Elmer, USA, model Optima 2000 DV). The initial water volume of the dilute compartment and the concentrate compartment were same, namely 2.5 liters. After the test, the water volume of the two compartments were measured to see whether water diffusion across the membranes happened.

5.2 Electrodialysis system setup

Figure S11 showed real pictures of the electrodialysis system used in this study to test membrane desalination performance. The components and their details as well as suppliers were summarized in Table S2.

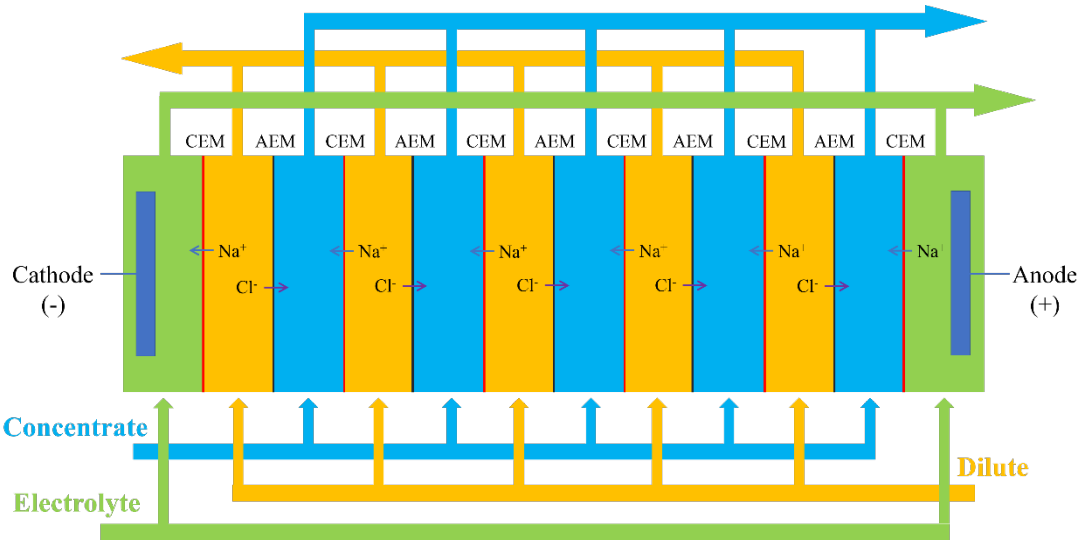


Figure S10. Schematic illustration of the electrodialysis cell. Salts were removed in the dilute compartment and were collected in the concentrate compartment.

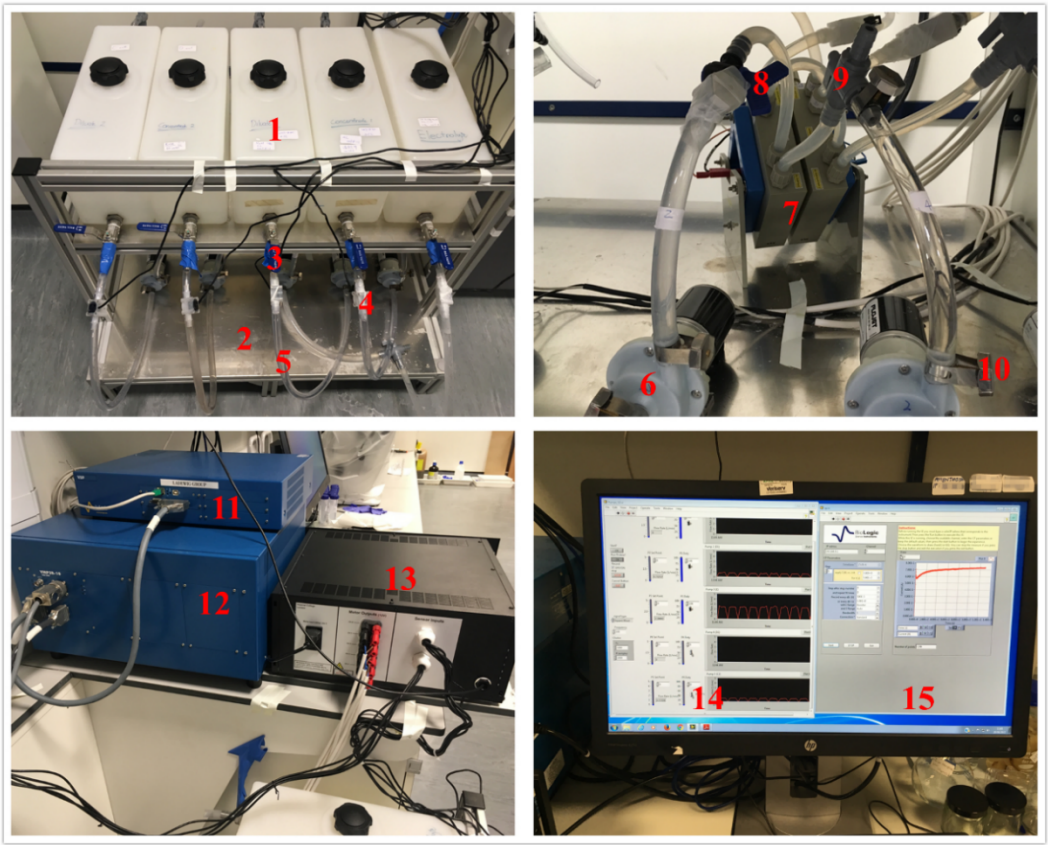


Figure S11. Real pictures of electrodialysis system. 1- Tank; 2- Framework; 3- Valve 1; 4- Flow meter; 5- Tubing; 6- Pump; 7- Electrodialysis cell; 8- Valve 2; 9- Valve 3; 10- Hose connector; 11- Potentiostat; 12- Current booster; 13- Control power interface unit; 14- Pump control and flow rate display panel; 15- Potentiostat control panel

Table S2. Components of the electrodialysis system

Component Name	Component details	Supplier
Pump	Xylem Totton Magnetic Coupling Centrifugal Pump, 23L/min, 12 V dc	RS Components
Flow meter	RS Pro, 0.05 → 10 L/min Flow Controller V10980	RS Components
Valve 1	RS Pro Manual Ball Valve Stainless Steel 1/2 in BSPP	RS Components
Valve 2	12mm Hose Tail Plastic Ball Valve Air-pro	Hoses Direct
Valve 3	Ball valve, 3-way, 1/2" barb, - PVC	Cole Palmer
Connecting fitting 1	RS Pro Stainless Steel Hexagon Bush 3/4in R(T) Male x 1/2in G(P) Female	RS Components
Connecting fitting 2	RS Pro Stainless Steel Hexagon Nipple 1/2in R(T) Male x 1/2in R(T) Male	RS Components
Connecting fitting 3	RS Pro Stainless Steel Hexagon Hose Nipple 1/2in R(T) Male / Male	RS Components
Tank	12 Litre Water Tanks (Natural)	Tanks Direct
Torque wrench	Mighty Torque Wrench - Black	Amazon
Wrench head	Stahlwille 540 Series Crow Foot Spanner Head, size 8 mm Chrome	RS Components
Tubing 1	1/4" PVC Tubing	Imperial College
Tubing 2	3/8" Silicone Tubing	Imperial College
Tape	PTFE Tape	Imperial College
Hose Connectors	Hose Connectors	Imperial College
Framework	Aluminium Framework	KJN
Control power interface unit	NA	National Instruments
Potentiostat	VSP	BioLogic
Current booster	VMP3B-10	BioLogic

5.3 Result and discussion

Real-time monitoring of flow rates of dilute, concentrate and electrolyte compartments was shown in Figure S12, Figure S13 and Figure S14, respectively. As revealed by these figures, the flow rates of the entire system were very stable. To be specific, the average flow rate of the dilute, concentrate and electrolyte compartments were 0.75 L/min, 0.73 L/min and 2.50 L/min, respectively. The flow rates of dilute compartment and concentrate compartment were nearly the same, which was an important condition since great difference in flow rate of these two compartments would generate pressure difference across membranes. Pressure difference was bad for membranes and should be avoided or reduced to the minimum.

The volume change in dilute and concentrate parts before and after electrodialysis test was summarized in Table S3. No volume changes occurred after the test, indicating that no or negligible water diffusion across the membrane took place. Also, as revealed by Figure S18 and Figure S19, both conductivity and sodium concentration in the dilute water decreased as time went on. In contrast, both conductivity and sodium concentration in the concentrate water increased as time went on. Therefore, the practicability of these membranes for water treatment/desalination was confirmed. One future research work is to improve desalination performance by reducing membrane resistance, since these membranes indicated high membrane resistance, as revealed by Figure S15 and Figure S16, where the current was not high enough even though the initial current was set to be 5 A.

Table S3. Volume change in dilute and concentrate parts before and after test

Compartment	Before test	After test
Dilute	2.5 L	2.5 L
Concentrate	2.5 L	2.5 L

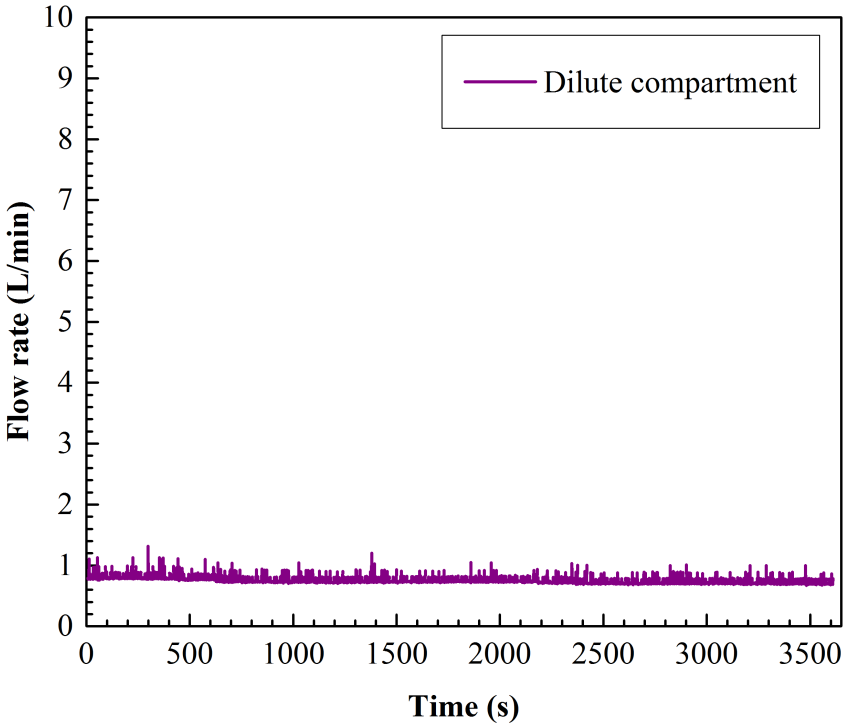


Figure S12. Real-time monitoring of flow rate of the dilute compartment.

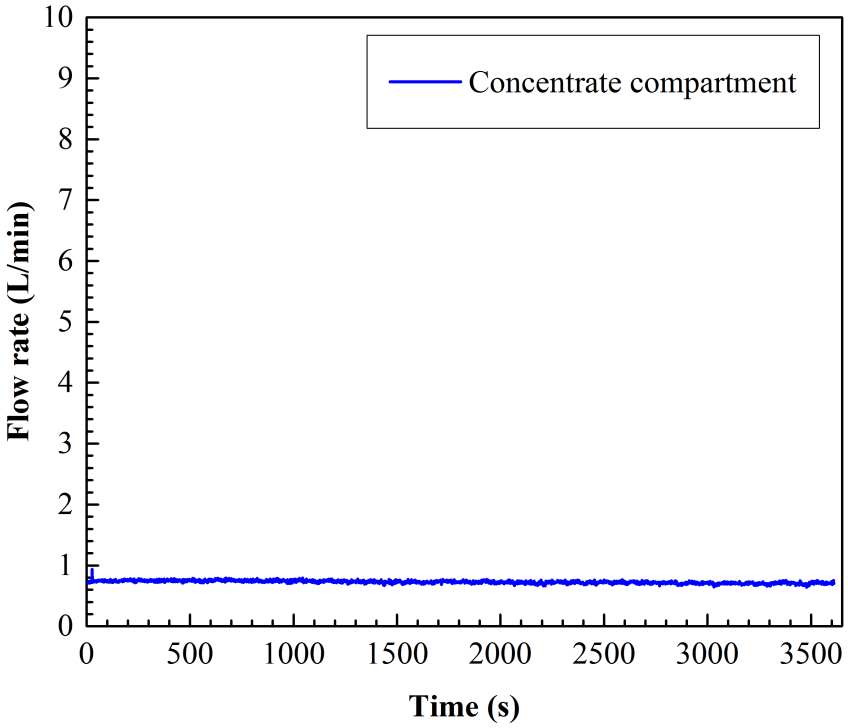


Figure S13. Real-time monitoring of flow rate of the concentrate compartment.

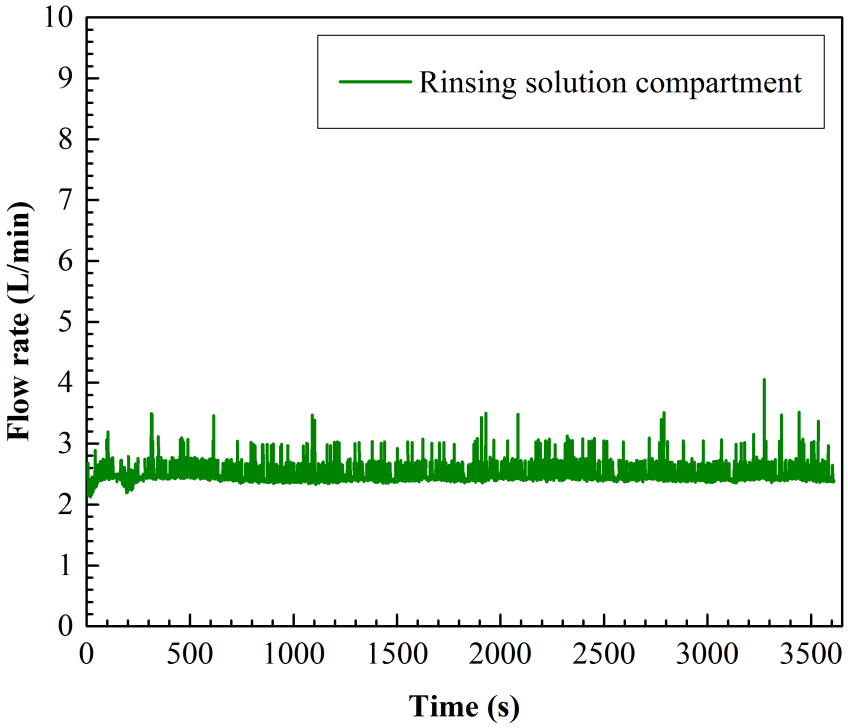


Figure S14. Real-time monitoring of flow rate of the dilute compartment.

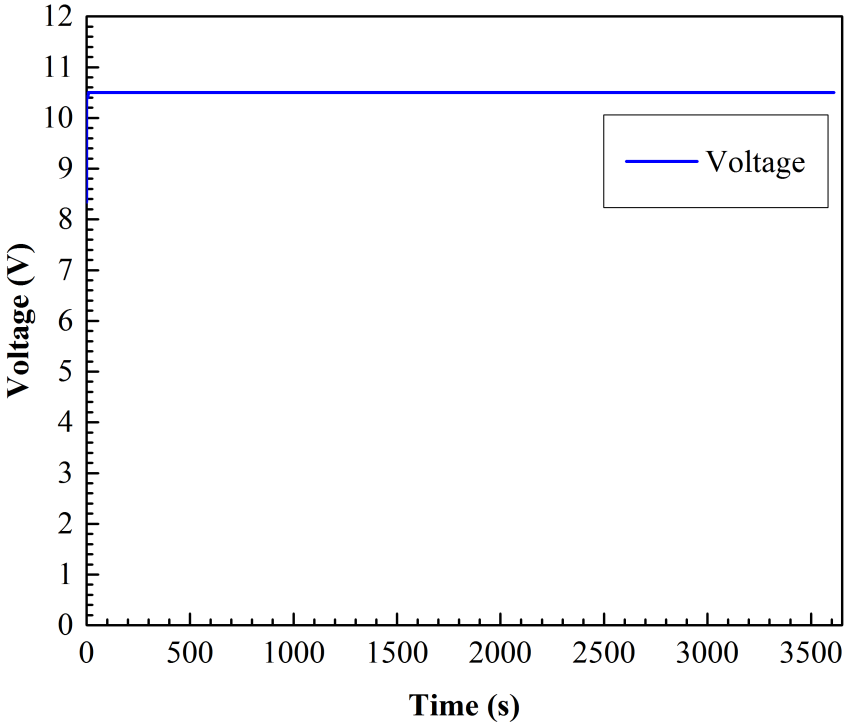


Figure S15. Real-time monitoring of voltage applied to the electrodialysis cell.

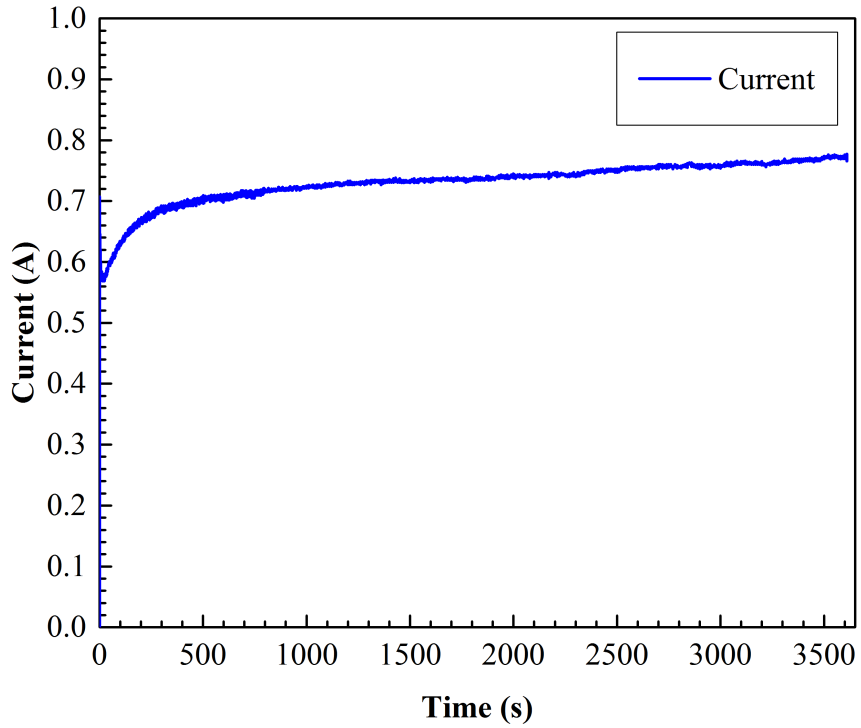


Figure S16. Real-time monitoring of current supplied to the electrodialysis cell.

Replicate Data: Calib Blank 1

Repl#	Analyte	Net Intensity	Corrected Intensity	Conc.	Calib. Units	Analysis Time
1	Na 589.592	-6891.4	-6891.4	[0.00]	mg/L	10:07:58
2	Na 589.592	-6824.0	-6824.0	[0.00]	mg/L	10:08:06
3	Na 589.592	-7128.2	-7128.2	[0.00]	mg/L	10:08:14

Mean Data: Calib Blank 1

Analyte	Mean Corrected Intensity	Std.Dev.	RSD	Conc.	Calib Units
Na 589.592	-6947.8	159.76	2.30%	[0.00]	mg/L

Replicate Data: 1

Repl#	Analyte	Net Intensity	Corrected Intensity	Conc.	Calib. Units	Analysis Time
1	Na 589.592	777503.7	784451.6	[5.0500]	mg/L	10:09:45
2	Na 589.592	768797.4	775745.2	[5.0500]	mg/L	10:09:48
3	Na 589.592	787201.4	794149.2	[5.0500]	mg/L	10:09:51

Mean Data: 1

Analyte	Mean Corrected Intensity	Std.Dev.	RSD	Conc.	Calib Units
Na 589.592	784782.0	9206.46	1.17%	[5.0500]	mg/L

Replicate Data: 2

Repl#	Analyte	Net Intensity	Corrected Intensity	Conc.	Calib. Units	Analysis Time
1	Na 589.592	1535765.1	1542713.0	[9.9925]	mg/L	10:11:24
2	Na 589.592	1563569.2	1570517.1	[9.9925]	mg/L	10:11:27
3	Na 589.592	1519100.0	1526047.9	[9.9925]	mg/L	10:11:30

Mean Data: 2

Analyte	Mean Corrected Intensity	Std.Dev.	RSD	Conc.	Calib Units
Na 589.592	1546426.0	22465.90	1.45%	[9.9925]	mg/L

Replicate Data: 3

Repl#	Analyte	Net Intensity	Corrected Intensity	Conc.	Calib. Units	Analysis Time
1	Na 589.592	3828802.2	3835750.1	[24.9045]	mg/L	10:13:01
2	Na 589.592	3802974.7	3809922.6	[24.9045]	mg/L	10:13:04
3	Na 589.592	3793786.0	3800733.9	[24.9045]	mg/L	10:13:07

Mean Data: 3

Analyte	Mean Corrected Intensity	Std.Dev.	RSD	Conc.	Calib Units
Na 589.592	3815468.8	18155.02	0.48%	[24.9045]	mg/L

Calibration Summary

Analyte	Stds.	Equation	Intercept	Slope	Curvature	Corr. Coef.	Reslope
Na 589.592	3	Lin Thru 0	0.0	153500	0.00000	0.999991	

Figure S17. Calibration of sodium standard solution for ICP measurement. The coefficient reached 0.99991, which was an excellent result.

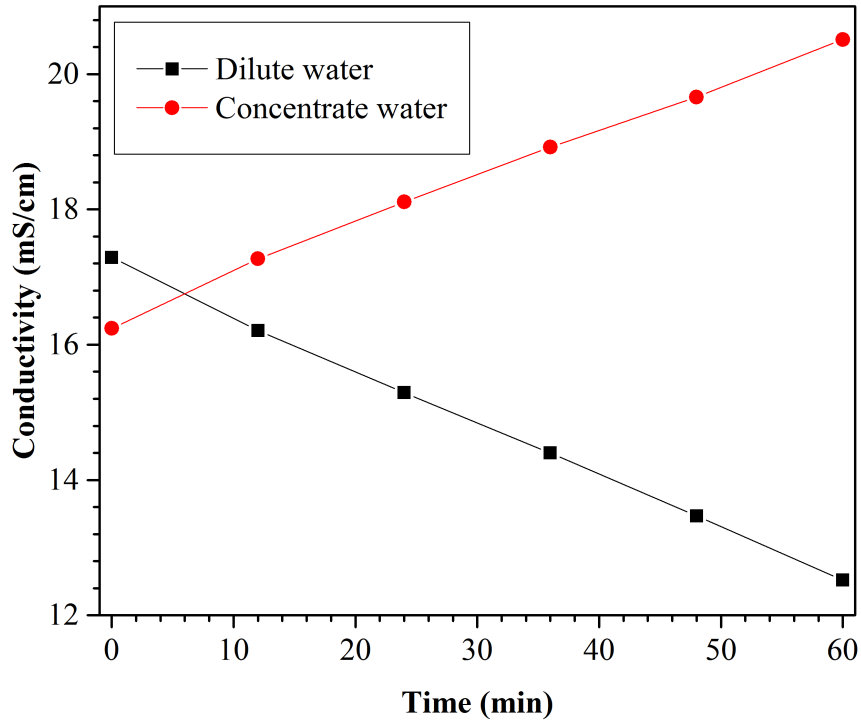


Figure S18. Changes of conductivity in dilute water and concentrate water with time

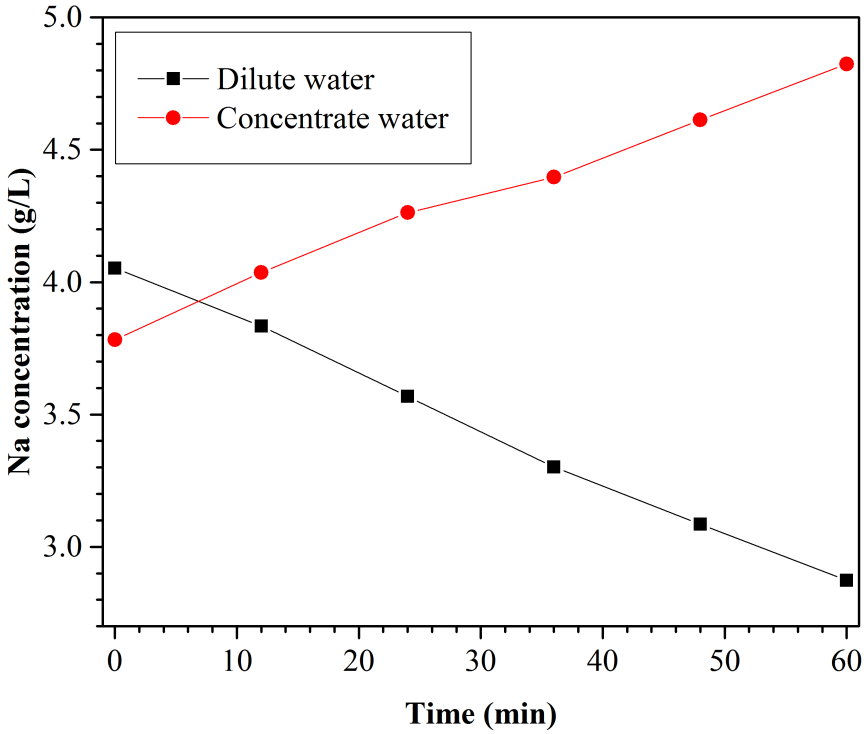


Figure S19. Changes of sodium concentration in dilute water and concentrate water with time

References

(1) Nam, S. E.; Kim, S. O.; Kang, Y.; Lee, J. W.; Lee, K. H. Preparation of Nafion/sulfonated Poly(phenylsilsesquioxane) Nanocomposite as High Temperature Proton Exchange Membranes. *J. Memb. Sci.* **2008**, *322* (2), 466–474.

(2) Almeida, N. E. De; Easton, E. B. Nafion/Sulfonated Silica Composite Membranes for PEM Fuel Cells. *ECS Trans.* **2010**, *28* (27), 29–38.

(3) Peckham, T. J.; Schmeisser, J.; Holdcroft, S. Relationships of Acid and Water Content to Proton Transport in Statistically Sulfonated Proton Exchange Membranes: Variation of Water Content via Control of Relative Humidity. *J. Phys. Chem. B* **2008**, *112* (10), 2848–2858.